Technical appendix: Physical climate projections

Robert E. Kopp[a,*], D.J. Rasmussen[b]

[a] *Department of Earth & Planetary Sciences and Rutgers Energy Institute, Rutgers University, Piscataway, NJ 08854, USA*
[b] *Rhodium Group, Oakland, CA, USA*

A.1. Temperature, precipitation and humidity projections

In constructing the ensemble of temperature and precipitation projections used in this analysis, we are trying to address two challenges. First, and preeminently, ensembles of opportunity like the Coupled Model Intercomparison Project (CMIP) ensembles are not probability distributions because they are arbitrarily compiled; any sampling from such a distribution would thus not be random and would likely undersample "tails" of the probability distribution (*Tebaldi and Knutti*, 2007). Yet while simple climate models like MAGICC (*Meinshausen et al.*, 2011) project probability distributions of global mean temperature change, they lack the spatial and temporal resolution needed to estimate climate risk, which downscaled global climate model (GCM) output can provide. We seek to combine these strengths. Second, traditional pattern scaling approaches estimate forced climate change but neglect unforced variability (e.g., *Mitchell*, 2003). The interactions between these two factors may play a significant role in the timing and amplitude of climate change damages, so here we estimate the combination and forced and unforced variability.

We start with an estimated probability distribution of global mean temperatures over time from a simple climate model, use this distribution to weight local projections of monthly temperature and precipitation from more complex global climate models and from surrogate models employed to ensure the tails of the probability distribution are represented, then use historical relationships to translate monthly values to daily values. We also construct a probabilistic estimate of wet-bulb temperatures based upon daily projections.

A.1.1. Global mean temperature

Projections of global mean temperature for the four representative concentration pathways (RCPs) were calculated using MAGICC6 (*Meinshausen et al.*, 2011) in probabilistic mode. MAGICC is a commonly-used simple climate model that represents the atmosphere, ocean, and carbon cycle at a hemispherically-averaged level. The distribution of input parameters for MAGICC that we employ has been constructed from a Bayesian analysis based upon historical observations (*Meinshausen et al.*, 2009; *Rogelj et al.*, 2012) and the climate sensitivity probability distribution of the Intergovernmental Panel on Climate Change's Fifth Assessment Report (AR5) (Figure A1) (*Collins et al.*, 2013).

The climate sensitivity probability distribution from AR5 is based on several lines of information. Observational, paleoclimatic, and feedback analysis evidence indicate 5th/17th/83rd percentiles of 1.0°C/1.5°C/4.5°C. Additional evidence from climate models suggests a 90th percentile of 6.0°C (*Collins et al.*, 2013).

For each RCP, we used 600 MAGICC model runs provided by M. Meinshausen (pers. comm.). The 5th/17th/83rd/90th percentiles of equilibrium climate sensitivity for these 600 runs are 1.5°C/1.6°C/4.9°C/ 5.9°C per CO_2 doubling. The differences in climate sensitivity between MAGICC and AR5 in part reflect sampling and in part the constraints needed to fit historical observations with the MAGICC model structure.

A.1.2. Global climate model output

Due to computational constraints, GCM results are often calculated with horizontal resolutions too coarse (e.g., around $2^o \times 2^o$) to assess climate change vulnerabilities and impacts at a spatial scale of interest to regional planners and policy makers. Additionally, GCM projections that are directly available from the CMIP5 archive contain systematic model biases that must be corrected before being employed to address climate impacts. In this study, projections of monthly average temperature, minimum daily temperature,

*Corresponding author
Email address: robert.kopp@rutgers.edu (Robert E. Kopp)

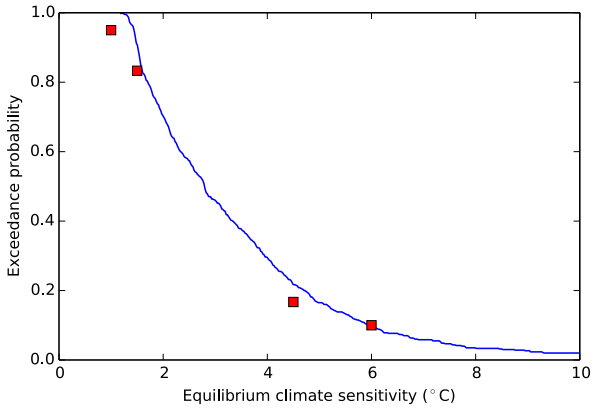

Figure A1: Survival function of climate sensitivities from MAGICC. Red squares indicate the statements made by AR5.

maximum daily temperature, and precipitation were obtained from a monthly bias-corrected and spatially-disaggregated (BCSD) archive derived from select CMIP5 models (*Brekke et al.*, 2013). For the continental United States, projections are disaggregated to 1/8 × 1/8 degree (∼14 km) horizontal resolution, while 1/2 × 1/2 degree (∼56 km) model output with global coverage over land only from is used to provide projections for Alaska and Hawaii. A detailed inventory of the models used with each RCP is shown in Table A1.

Rather than use the absolute model projections of temperature and precipitation, we assume that the models are best at projecting changes from a baseline period from their own historical climate estimates, here selected as 1981–2010. Model projections are then mapped and added to observed temperature and precipitation normals (1981–2010) at stations from the Global Historical Climatology Network (GHCN) (*Arguez et al.*, 2012) (`http://go.usa.gov/KmqH`). The GHCN data set is a database of meteorological variables measured daily worldwide and is the most comprehensive set of climate data within the United States. The use of station-level normals accounts for local meteorological phenomena, such as the urban heat island effect and land-sea interaction, that are not well reproduced by the gridded BCSD model output. Only GHCN stations that met the strictest of the National Climatic Data Center's data completion requirements for the 30-yr monthly climate normals definitions were used (2,688 sites for temperature, 2,722 sites for precipitation).

A.1.3. Pattern fitting

We regard the output of each model as the sum of forced climate change and unforced climate variability. We further assume that the forced climate change can be approximated as linear in the long-term (30-year) running average of global mean temperature. Accordingly, for each CMIP5 model and scenario i and each at station j, we fit the changes from the 1981–2010 reference levels for seasonal temperature and precipitation to the linear model

$$y_{i,j}(\Delta T, t) = \hat{k}_{i,j}\Delta T + b_{i,j} + \epsilon_{i,j}(t) \tag{A1}$$

following *Mitchell* (2003). Here, ΔT is the running-average change in global mean temperature relative to the reference period (1981–2010), $\hat{k}$ is the estimated seasonal pattern, $\hat{k}\Delta T$ is the estimated forced climate change, $b_{i,j}$ is the y-intercept and $\epsilon(t)$ is an estimated temporal pattern of unforced variability. In our analysis, we use a single realization of unforced variability from each CMIP5 model. Figure A2 shows an example regression for one particular model and scenario (GFDL-CM3 under RCP 8.5) at New York City for summertime monthly mean temperature and daily precipitation rate.

A.1.4. Probability weighting

We divide the unit interval $[0, 1]$ into ten bins, with a somewhat higher density of bins at the tails of the interval. (Specifically, the bins are centered at the 4th, 10th, 16th, 30th, 50th, 70th, 84th, 90th, 94th, and 99th percentiles.) The quantiles of global mean temperature change corresponding to the bounds and center

Table A1: CMIP5 models included in temperature and precipitation projections

Model	RCP 8.5	RCP 6.0	RCP 4.5	RCP 2.6
access1-0	x		x	
access1-3	x		x	
bcc-csm1-1	x	x	x	x
bcc-csm1-1-m	x		x	
bnu-esm	x		x	x
canesm2	x		x	x
ccsm4	x	x	x	x
cesm1-bgc	x		x	
cesm1-cam5	x	x	x	x
cmcc-cm	x		x	
cnrm-cm5	x		x	
csiro-mk3-6-0	x	x	x	x
fgoals-g2	x		x	x
fio-esm	x	x	x	
gfdl-cm3	x	x	x	x
gfdl-esm2g	x	x	x	x
gfdl-esm2m	x	x	x	
giss-e2-h-cc			x	
giss-e2-r	x	x	x	x
giss-e2-r-cc			x	
hadgem2-ao	x	x	x	x
hadgem2-cc	x		x	
hadgem2-es	x	x	x	x
inmcm4	x		x	
ipsl-cm5a-lr	x	x	x	x
ipsl-cm5a-mr	x	x	x	x
ipsl-cm5b-lr	x		x	
miroc-esm	x	x	x	x
miroc-esm-chem	x	x	x	x
miroc5	x	x	x	x
mpi-esm-lr	x		x	x
mpi-esm-mr	x		x	x
mri-cgcm3	x		x	x
noresm1-m	x	x	x	x
noresm1-me	x	x	x	x

of each bin are taken from the MAGICC6 output. CMIP5 model output is categorized into bins based on the projected change in global mean temperature from 1981–2010 to 2081–2099.

In bins, primarily at the tail of the distribution, not represented by at least 2 CMIP5 models, we generate model surrogates sufficient to bring the number of models plus surrogates to two. To generate a model surrogate, we take the global mean temperature projection from MAGICC output corresponding to the central quantile of the bin. If there is no CMIP5 output in the bin, we pick two models with global mean temperature projections close to the bin, such that one model pattern reflects a large net increase in contiguous US (CONUS) precipitation with temperature and one reflect a net decrease or lesser increase in CONUS precipitation with temperature. If there is a single CMIP5 model in the bin, we pick a single model with a precipitation pattern complementing the one in the bin. We then use the patterns from the selected models to scale the global mean temperature projection and add the residuals from the same models, generating a surrogate model that includes both forced change and unforced variability. A table of the models and surrogate models used, along with the spatial patterns of temperature and precipitation change, is provided in Tables A2–A5 and Figures A6–A7.

In the final probability distribution, the models and surrogates in a bin are weighted equally such that the total weight of the bin corresponds to the target distribution for 2081–2099 temperature. For example, if there are four models in the bin centered at the 30th percentile and stretching from the 20th to the 40th percentiles, each will be assigned a probability of $20\%/4 = 5\%$. Thus the projected distribution for global mean temperature approximates the target (Figure A3).

For models that end in 2100, we extend projections to 2200 by assuming that global mean temperature beyond 2100 follows the quantile of the MAGICC output that corresponds to that model's position in the

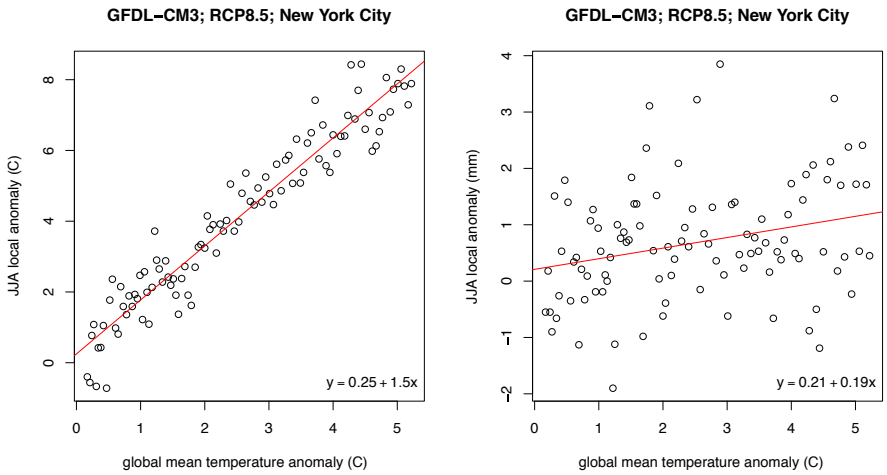

Figure A2: Left: Local summer (June-July-August) temperature anomaly at Central Park, New York City, versus global mean temperature anomaly for the GFDL-CM3 model under RCP 8.5. Right: as for Left, but for daily precipitation rate (mm/day).

2081–2099 average. We apply the model's own pattern of forced change and use residuals (i.e. unforced variability) that are equal to the residuals from 2000 to 2099, run backwards to preserve continuity.

To assess the effect of the probability weighting on our results, we present in Tables A6 to A13 a comparison of our projections with model weights and surrogate models to those based simply on the unweighted distribution of results from CMIP5. Table A6 shows the sensitivity of regional average annual temperatures under RCP 8.5 in a weighted and unweighted scheme. The largest differences between methods occurs at the end of the 21st century in the 5–95th percentile interval. The differences between unweighted and weighted range from 1.3°C in Hawaii to nearly 3.0°C over Alaska. Differences in seasonal precipitation totals are presented in Tables A7 to A10, and, in general, show less of a divergence between weighting schemes compared to annual average temperature. Differences in extreme heat/humidity days (Chapter 4) are presented in Tables A11 to A13. The largest differences between weighting schemes occurs in the most extreme conditions (ACP Humid Heat Stroke Index Category IV).

A.1.5. Daily projections

Both GCM output and surrogate output are treated at the monthly average level. To generate daily temperature and precipitation, we assume that relationship between the monthly means and the daily values come from a stationary distribution (e.g. *Wood et al.*, 2002), which is the standard approach for BCSD downscaling. We randomly assign each future year to a historical year between 1981–2010. Monthly averages are mapped to daily values from the GHCN stations using the additive relationship (for temperature) or multiplicative relationship (for precipitation) from that historical year. Where daily observations are missing from the 30-year historical record, we fill in the missing days and months using relationships between daily and monthly values from gridded datasets and between the climatological 30-year normal value at the GHCN station. A gridded observational data set (*Maurer et al.*, 2002) and the North American Regional Reanalysis (NARR) (*Mesinger et al.*, 2006) are used to provide the daily values for the continental United States and for Alaska and Hawaii, respectively. Where daily precipitation projections exceed twice the historical daily maximum and ten times the model's mean daily precipitation rate for the month, we invoke a "spill over" routine that evenly distributes two-thirds of the incident daily precipitation to the nearest adjacent two days

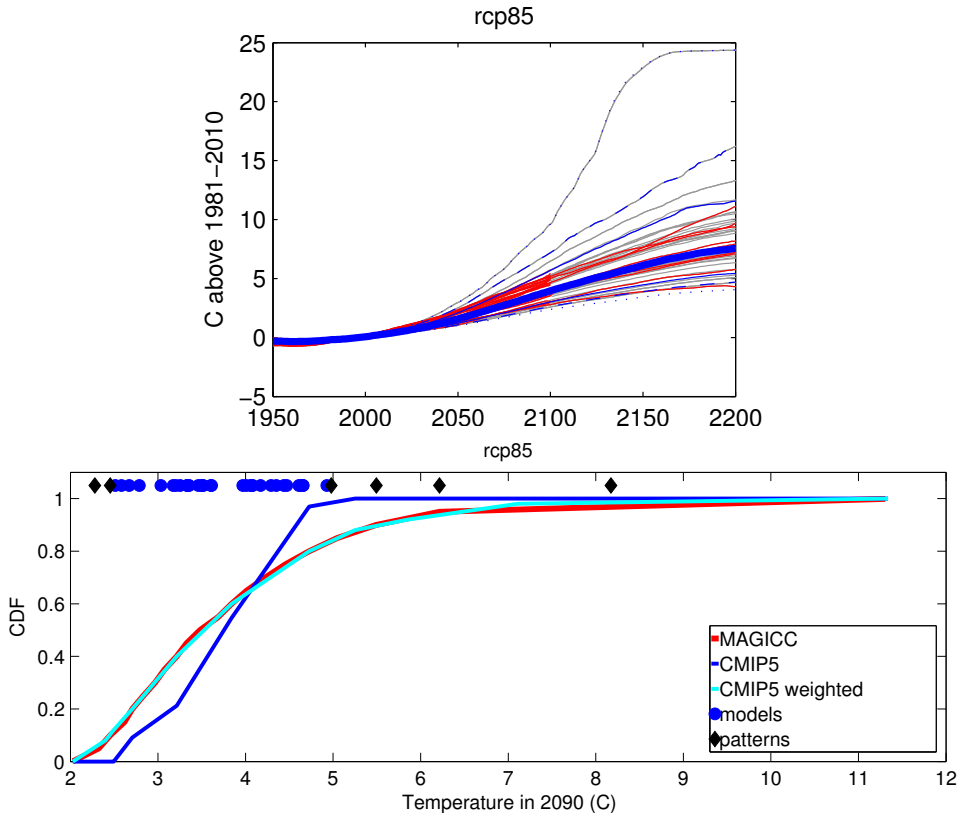

Figure A3: (Top) Global mean temperature trajectories for RCP 8.5 from MAGICC (blue), CMIP5 model output (red) and model surrogates (grey). Heavy blue = median, light blue = 17th/83rd percentile, dashed blue = 5th/95th percentile, dotted blue = 1st/99th percentiles. (Bottom) The distribution of 2081–2099 global mean temperature for RCP 8.5. Blue dots = CMIP5 output, black diamonds = model surrogates, blue curve = CMIP5 model output CDF, red curve = MAGICC projection, cyan curve = CMIP5 models and model surrogates weighted to align with MAGICC projections.

within the month. Daily maximum and minimum temperatures for Alaska and Hawaii were calculated from 3-hourly NARR data. For the rare case when the daily downscaled $T_{min} < T_{avg} < T_{max}$ is not satisfied, T_{min} and T_{max} are approximated as T_{avg} - 2.5 K and T_{avg} + 2.5 K, respectively. An example of the daily weather generation is shown in Figure A4.

A.1.6. Wet-bulb temperatures

At each GHCN site, we estimate a relationship between dry-bulb and wet-bulb temperature and the associated error with (1) a simple linear model and (2) a piecewise linear model with a single breakpoint. The model with the smallest Bayesian information criterion (BIC) is used. The simple linear model is of the form:

$$T_w(T) \quad = \quad b_0 + \beta_0 T_d + \epsilon. \tag{A2}$$

The piecewise linear model is of the form:

$$T_w(T) \quad = \quad b_1 + \beta_1 \min(T_d, T_0) + \beta_2 \max(0, T_d - T_0) + \epsilon. \tag{A3}$$

Here, T_w is the wet bulb temperature, T_d the dry bulb temperature, b_i are y-intercepts, β_i are slopes, and T_0 is the breakpoint. Errors ϵ are assumed to come from a stationary normal distribution, $\epsilon \sim N(0, \sigma^2)$. The model is fit to historical (1981–2010) maximum daily wet-bulb temperatures calculated using the Wobus method (*Doswell et al.*, 1982; *Marsh and Hart*, 2012) from 3-hourly 2-m temperature, 2-m dew point temperature and pressure from NARR. Examples are shown in Figure A5. While commonly used, the Wobus method

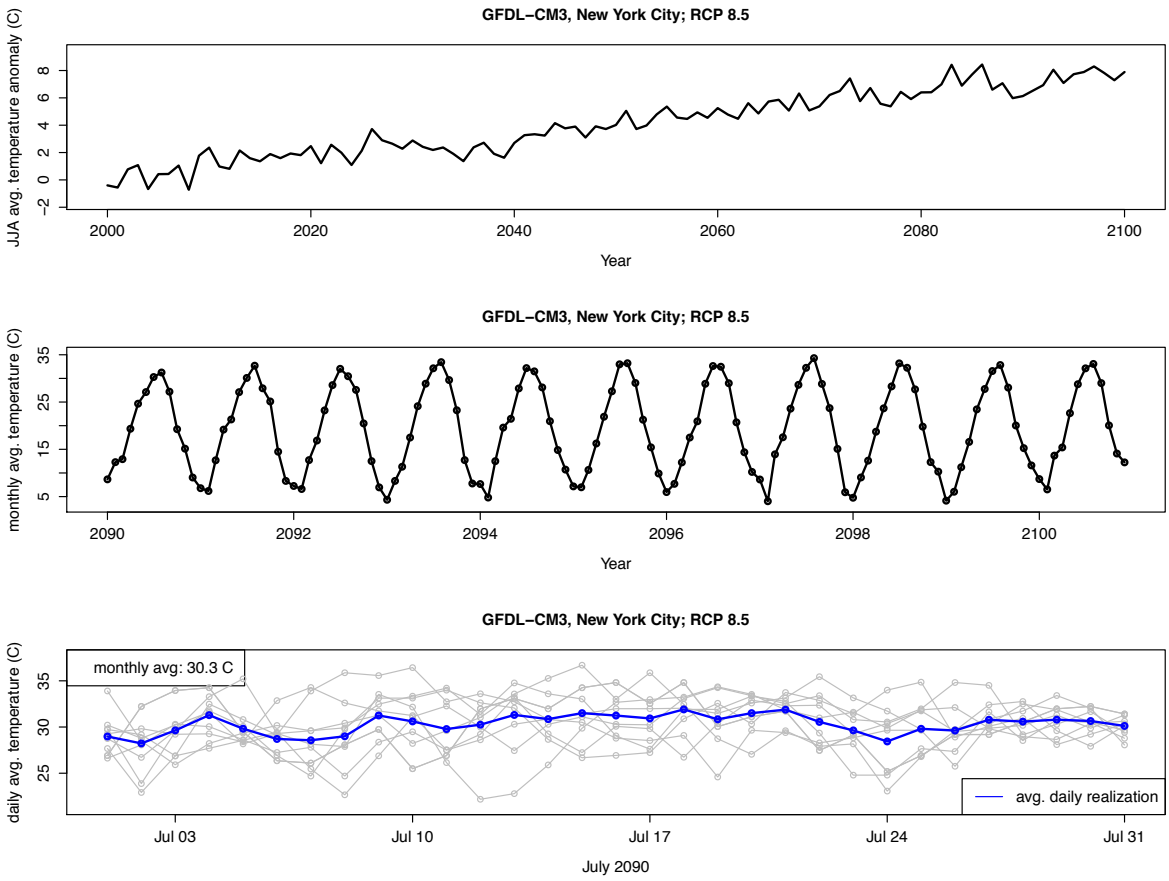

Figure A4: Example of data generation from one CMIP5 model (GFDL-CM3) and scenario (RCP 8.5) at Central Park, New York, showing (a) seasonal projections for the century (relative to 1981–2010) , (b) monthly projections for 2091–2100 and (c) 10 independent daily weather projections for average temperature in July in 2099. The blue line is the average of all 10 projections and is equal to the July 2099 monthly average.

does introduce small errors compared to more precise calculations (*Davies-Jones*, 2008). These errors are generally < 1 K, and do not significantly affect the ACP Humid Heat Stroke index introduced in Chapter 4.

The regression provides the distribution of T_w conditional on T_d for the baseline climatology. To account for the effects of climate change, we shift the conditional distribution upward by $\beta_0 \Delta T_f$, where ΔT_f is the local forced summertime temperature change given by $\hat{k}\Delta T$ in equation A1. In particular, we use the relationship

$$T_w(T_d, \Delta T_f) \quad = \quad T_w(T_d - \Delta T_f) + \beta_0 \Delta T_f \tag{A4}$$

to generate estimates of future wet bulb temperatures. Note that, for cases where the simple linear model best captures the distribution, this expression reduces to that model.

The extrapolation of the historical relationship between wet-bulb and dry-bulb temperatures effectively assumes that the distribution of relative humidities remains near constant. In fact, because the land warms faster than the ocean, relative humidity over land is expected to decrease in a warmer climate (*Sherwood and Fu*, 2014). The failure of our historically-based method to account for this shift may result in a slight upward bias in projected wet-bulb temperatures in areas not in proximity to large bodies of water such as the oceans or the Great Lakes.

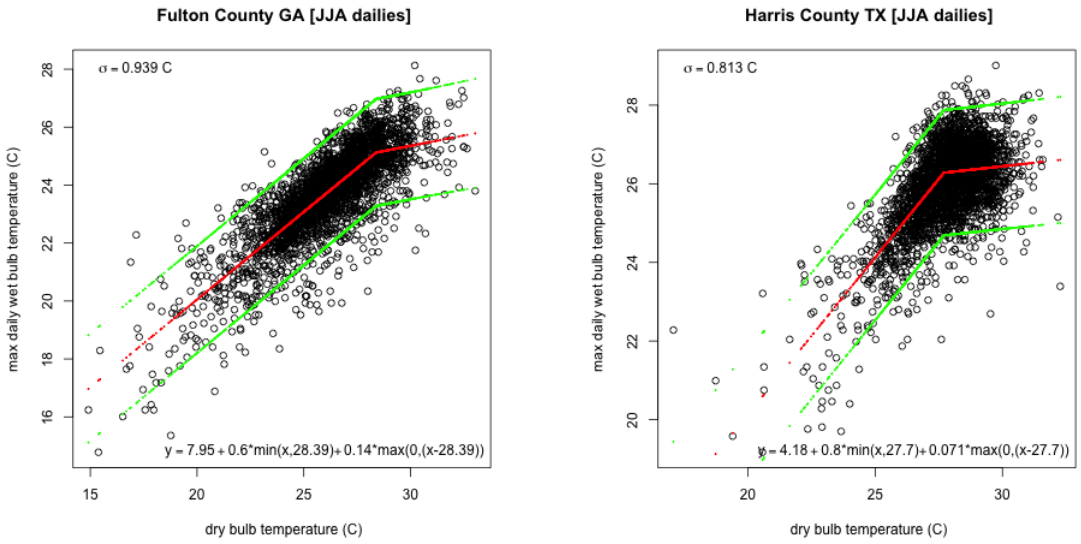

Figure A5: Fit of historical summertime (June-July-August) daily maximum wet-bulb temperatures to daily average temperature at Fulton County, Georgia and Harris County, Texas. Equations are shown for the best-fit piecewise linear model. The standard deviation from the best-fit model is also shown.

Table A2: Selected patterns and probability weights used for RCP 2.6

Quantile	Model	Weight	2080–2099 global ΔT (C)	2080–2099 CONUS ΔP (%)
0.00	gfdl-esm2g	0.04	0.25	-1.41
0.04	scaled fio-esm	0.04	0.39	-0.70
0.10	giss-e2-r	0.02	0.46	2.42
0.10	scaled giss-e2-r	0.02	0.46	2.39
0.16	scaled fgoals-g2	0.04	0.52	2.99
0.20	fgoals-g2	0.04	0.58	3.34
0.30	scaled mpi-esm-lr	0.10	0.64	3.38
0.40	mpi-esm-lr	0.10	0.78	4.13
0.40	mpi-esm-mr	0.03	0.78	2.57
0.43	bcc-csm1-1	0.03	0.82	0.33
0.46	noresm1-m	0.03	0.84	0.59
0.47	ccsm4	0.03	0.86	5.01
0.55	noresm1-me	0.03	0.94	6.42
0.55	mri-cgcm3	0.03	0.92	3.78
0.63	miroc5	0.04	1.03	4.11
0.65	ipsl-cm5a-mr	0.04	1.07	-1.39
0.66	hadgem2-ao	0.04	1.08	-0.23
0.68	bnu-esm	0.04	1.13	1.02
0.76	ipsl-cm5a-lr	0.04	1.25	6.10
0.82	hadgem2-es	0.02	1.40	9.26
0.84	cesm1-cam5	0.02	1.46	13.56
0.85	csiro-mk3-6-0	0.02	1.45	10.41
0.85	canesm2	0.02	1.47	7.79
0.90	scaled miroc-esm-chem	0.02	1.62	7.43
0.91	miroc-esm	0.02	1.65	7.25
0.93	miroc-esm-chem	0.03	1.69	7.78
0.97	gfdl-cm3	0.03	1.92	6.14
0.99	scaled hadgem2-es	0.01	2.18	14.41
0.99	scaled miroc-esm-chem	0.01	2.18	10.05

Table A3: Selected patterns and probability weights used for RCP 4.5

Quantile	Model	Weight	2080–2099 global ΔT (C)	2080–2099 CONUS ΔP (%)
0.04	scaled gfdl-esm2g	0.04	0.93	4.63
0.07	gfdl-esm2g	0.04	0.99	4.93
0.09	fio-esm	0.02	1.03	1.64
0.10	scaled gfdl-esm2m	0.02	1.03	2.37
0.17	gfdl-esm2m	0.03	1.17	2.70
0.18	giss-e2-r-cc	0.03	1.17	1.98
0.20	giss-e2-r	0.03	1.19	2.02
0.21	inmcm4	0.05	1.21	7.65
0.25	fgoals-g2	0.05	1.31	2.89
0.29	giss-e2-h-cc	0.05	1.36	6.51
0.37	bcc-csm1-1-m	0.05	1.49	-4.01
0.41	cesm1-bgc	0.02	1.56	4.52
0.42	bcc-csm1-1	0.02	1.57	4.23
0.44	mpi-esm-lr	0.02	1.62	5.52
0.45	noresm1-m	0.02	1.60	5.92
0.45	ipsl-cm5b-lr	0.02	1.62	9.24
0.45	ccsm4	0.02	1.62	6.16
0.45	mri-cgcm3	0.02	1.63	10.28
0.46	noresm1-me	0.02	1.67	1.67
0.48	mpi-esm-mr	0.02	1.68	4.53
0.48	miroc5	0.02	1.71	0.34
0.58	cnrm-cm5	0.02	1.88	6.97
0.70	access1-3	0.02	2.10	9.22
0.71	cmcc-cm	0.02	2.14	0.21
0.71	bnu-esm	0.02	2.13	1.06
0.72	ipsl-cm5a-lr	0.02	2.17	-2.60
0.74	access1-0	0.02	2.21	3.10
0.74	ipsl-cm5a-mr	0.02	2.23	-4.01
0.74	csiro-mk3-6-0	0.02	2.24	13.46
0.77	canesm2	0.02	2.30	13.32
0.78	hadgem2-cc	0.02	2.31	2.77
0.78	cesm1-cam5	0.02	2.30	6.44
0.79	hadgem2-ao	0.02	2.36	-1.42
0.82	miroc-esm	0.02	2.46	4.19
0.84	hadgem2-es	0.02	2.55	8.15
0.85	miroc-esm-chem	0.02	2.53	11.40
0.88	gfdl-cm3	0.02	2.70	10.00
0.90	scaled miroc-esm-chem	0.02	2.80	12.58
0.90	scaled hadgem2-ao	0.02	2.80	-1.68
0.95	scaled miroc-esm-chem	0.03	3.23	14.51
0.95	scaled hadgem2-ao	0.03	3.23	-1.94
0.99	scaled miroc-esm-chem	0.01	4.12	18.54
0.99	scaled hadgem2-ao	0.01	4.12	-2.47

Table A4: Selected patterns and probability weights used for RCP 6.0

Quantile	Model	Weight	2080–2099 global ΔT (C)	2080–2099 CONUS ΔP (%)
0.04	scaled gfdl-esm2m	0.04	1.31	2.22
0.04	scaled fio-esm	0.04	1.31	-0.78
0.10	scaled gfdl-esm2m	0.02	1.42	2.42
0.10	scaled fio-esm	0.02	1.42	-0.85
0.15	gfdl-esm2g	0.04	1.50	2.40
0.18	fio-esm	0.04	1.56	-0.93
0.24	giss-e2-r	0.07	1.62	3.23
0.25	gfdl-esm2m	0.07	1.66	2.82
0.36	noresm1-m	0.07	1.85	7.76
0.41	noresm1-me	0.05	1.94	4.27
0.43	bcc-csm1-1	0.05	1.96	5.09
0.44	miroc5	0.05	1.98	1.39
0.49	ccsm4	0.05	2.11	8.42
0.65	csiro-mk3-6-0	0.04	2.41	1.45
0.67	hadgem2-ao	0.04	2.49	-1.54
0.69	ipsl-cm5a-lr	0.04	2.55	-1.53
0.72	ipsl-cm5a-mr	0.04	2.61	-5.75
0.78	cesm1-cam5	0.04	2.76	17.36
0.82	miroc-esm	0.02	2.93	10.84
0.85	miroc-esm-chem	0.02	3.03	9.40
0.86	hadgem2-es	0.02	3.06	6.42
0.87	gfdl-cm3	0.02	3.10	11.80
0.90	scaled miroc-esm-chem	0.02	3.25	10.08
0.90	scaled hadgem2-es	0.02	3.25	6.83
0.95	scaled miroc-esm-chem	0.03	3.79	11.74
0.95	scaled hadgem2-es	0.03	3.79	7.95
0.99	scaled miroc-esm-chem	0.01	4.47	13.87
0.99	scaled hadgem2-es	0.01	4.47	9.40

Table A5: Selected patterns and probability weights used for RCP 8.5

Quantile	Model	Weight	2080–2099 global ΔT (C)	2080–2099 CONUS ΔP (%)
0.04	scaled giss-e2-r	0.04	2.26	8.37
0.04	scaled inmcm4	0.04	2.26	1.58
0.10	scaled giss-e2-r	0.02	2.43	9.00
0.10	scaled inmcm4	0.02	2.43	1.70
0.12	giss-e2-r	0.03	2.50	9.26
0.14	inmcm4	0.03	2.58	1.81
0.18	gfdl-esm2m	0.03	2.64	5.29
0.22	gfdl-esm2g	0.05	2.77	7.20
0.33	fgoals-g2	0.05	3.03	1.52
0.39	noresm1-m	0.05	3.14	6.60
0.40	mri-cgcm3	0.05	3.19	13.38
0.43	bcc-csm1-1-m	0.02	3.24	4.85
0.45	miroc5	0.02	3.31	-0.33
0.46	ipsl-cm5b-lr	0.02	3.33	9.32
0.46	noresm1-me	0.02	3.32	2.98
0.47	bcc-csm1-1	0.02	3.34	2.00
0.50	fio-esm	0.02	3.42	6.50
0.50	cnrm-cm5	0.02	3.47	11.10
0.51	cesm1-bgc	0.02	3.48	6.61
0.51	mpi-esm-mr	0.02	3.52	5.63
0.53	mpi-esm-lr	0.02	3.55	5.33
0.53	ccsm4	0.02	3.59	5.39
0.64	access1-3	0.01	3.96	15.44
0.65	csiro-mk3-6-0	0.01	3.97	11.92
0.66	hadgem2-ao	0.01	4.04	2.02
0.66	access1-0	0.01	4.05	0.81
0.67	cesm1-cam5	0.01	4.04	10.92
0.69	cmcc-cm	0.01	4.14	5.39
0.71	bnu-esm	0.01	4.27	3.41
0.73	ipsl-cm5a-mr	0.01	4.36	-10.46
0.75	canesm2	0.01	4.41	22.06
0.75	ipsl-cm5a-lr	0.01	4.43	-5.31
0.78	hadgem2-cc	0.01	4.60	5.97
0.78	gfdl-cm3	0.01	4.61	12.92
0.78	miroc-esm	0.01	4.62	5.09
0.78	hadgem2-es	0.01	4.63	6.94
0.83	miroc-esm-chem	0.04	4.90	4.90
0.84	scaled miroc-esm-chem	0.04	4.93	4.93
0.90	scaled gfdl-cm3	0.02	5.45	15.26
0.90	scaled miroc-esm-chem	0.02	5.45	5.45
0.95	scaled gfdl-cm3	0.03	6.20	17.35
0.95	scaled miroc-esm-chem	0.03	6.20	6.20
0.99	scaled gfdl-cm3	0.01	8.07	22.59
0.99	scaled miroc-esm-chem	0.01	8.07	8.07

Table A6: Average annual temperature anomaly (°C) for both weighted and un-weighted distributions

RCP 8.5			2040–2059 anomaly (Δ°C)			2080–2099 anomaly (Δ°C)		
Region	1981–2010 (°C)	Method	50	17–83	5–95	50	17–83	5–95
CONUS	11.9	unweighted	4.4	3.1–5.5	2.6–6.4	9.2	6.4–10.6	5.9–12.4
		weighted	4.4	2.6–5.8	2.5–6.4	9.4	6.1–12.4	5.7–14.3
Northeast	8.8	unweighted	4.5	3.5–5.6	2.9–6.9	9.3	6.8–11.4	6.4–12.7
		weighted	4.5	3.0–6.4	2.4–7.0	9.3	6.6–12.8	5.5–15.9
Southeast	16.8	unweighted	3.9	2.9–4.6	2.3–5.3	8.0	6.4–9.4	4.9–10.7
		weighted	3.9	2.4–5.1	2.0–5.7	8.1	5.4–10.8	4.9–13.1
N. Great Plains	7.2	unweighted	4.7	3.1–5.9	2.2–7.0	9.6	6.6–11.1	5.7–13.5
		weighted	4.7	2.9–6.4	2.5–7.0	9.7	6.0–13.5	5.7–15.1
S. Great Plains	16.8	unweighted	4.5	3.0–5.1	2.6–5.7	8.8	6.9–10.4	6.0–11.4
		weighted	4.5	2.9–5.2	2.4–6.0	8.9	6.2–11.4	5.8–13.9
Midwest	9	unweighted	4.9	3.4–6.0	2.9–7.4	9.7	6.8–11.7	6.2–14.2
		weighted	5.0	3.0–6.8	2.8–7.4	10.2	6.3–14.2	6.1–15.7
Northwest	8.8	unweighted	4.1	3.0–5.3	2.3–6.5	8.1	6.1–10.7	5.8–12.2
		weighted	4.2	2.3–6.0	2.2–6.6	8.1	5.8–12.2	4.9–13.6
Southwest	12.4	unweighted	4.5	3.2–5.5	2.6–6.2	8.6	6.9–10.7	6.2–12.5
		weighted	4.5	2.7–5.7	2.4–6.2	8.6	6.4–12.5	5.9–14.4
Alaska	-1.7	unweighted	5.7	3.9–7.2	3.6–8.6	10.5	7.7–14.8	6.6–16.2
		weighted	5.8	3.9–8.0	2.4–9.1	11.4	7.7–16.3	6.6–19.1
Hawaii	23.6	unweighted	2.5	1.8–3.4	1.6–4.0	5.0	4.1–7.4	3.7–8.1
		weighted	2.6	1.6–3.6	1.2–4.4	5.2	3.7–7.7	3.3–9.4

Table A7: Weighted and unweighted regional average winter precipitation change (Δ%)

DJF RCP 8.5			2040–2059 change (Δ%)			2080–2099 change (Δ%)		
Region	1981–2010 (mm)	Method	50	17–83	5–95	50	17–83	5–95
CONUS	159.7	unweighted	7.0	-1.4–10.3	-3.8–15.5	11.2	1.6–24.2	-9.5–29.2
		weighted	2.5	-2.0–10.1	-2.9–15.5	7.3	-1.4–21.4	-1.7–25.6
Northeast	228.4	unweighted	12.6	3.1–17.5	-14.5–23.9	23.3	8.6–33.9	1.7–44.4
		weighted	4.4	-1.4–16.7	-2.5–23.9	15.8	-0.8–33.0	-1.8–37.8
Southeast	323.4	unweighted	4.0	-3.4–11.4	-12.9–14.5	3.8	-6.3–21.9	-22.9–32.7
		weighted	-0.3	-3.4–9.8	-9.3–14.5	-0.9	-2.3–16.2	-14.9–31.4
N. Great Plains	40.6	unweighted	19.7	8.0–27.6	-11.6–37.6	37.8	24.2–55.4	13.9–70.6
		weighted	17.5	-1.1–27.6	-2.6–37.6	33.7	-0.2–49.7	-1.6–70.6
S. Great Plains	121.6	unweighted	-0.9	-12.4–9.4	-13.4–12.6	-2.3	-18.7–15.9	-34.6–24.2
		weighted	-1.5	-11.0–7.0	-13.0–11.7	-1.4	-11.8–10.5	-25.9–22.8
Midwest	135.0	unweighted	9.9	3.2–17.3	-7.0–28.0	21.7	10.1–35.1	-11.1–39.8
		weighted	6.7	-1.5–14.3	-6.1–28.0	17.0	-0.5–32.3	-1.4–35.5
Northwest	241.6	unweighted	9.3	-1.7–14.9	-13.4–19.9	13.7	-1.4–26.5	-15.1–42.1
		weighted	4.0	-2.1–12.3	-10.7–19.9	5.5	-2.4–26.5	-14.4–42.1
Southwest	110.4	unweighted	5.5	-8.8–15.5	-14.9–30.3	13.3	-5.2–37.5	-19.3–54.8
		weighted	-0.9	-6.2–12.8	-14.9–30.3	1.2	-2.7–36.0	-19.3–51.6
Alaska	105.8	unweighted	12.1	3.2–21.2	0.4–27.7	30.6	15.0–42.1	5.6–65.2
		weighted	6.0	-1.5–20.6	-1.6–25.0	15.5	0.3–40.4	-1.4–65.2
Hawaii	601.1	unweighted	-7.1	-16.9–5.2	-21.2–10.2	-3.9	-13.8–8.4	-28.3–28.0
		weighted	-3.3	-15.6–2.3	-21.2–5.8	-3.1	-13.0–6.7	-28.3–16.4

Table A8: Weighted and unweighted regional average spring precipitation change (Δ%)

MAM RCP 8.5			2040–2059 change (Δ%)			2080–2099 change (Δ%)		
Region	1981–2010 (mm)	Method	50	17–83	5–95	50	17–83	5–95
CONUS	196.1	unweighted	6.6	2.6–12.5	-3.2–16.1	10.7	2.2–17.6	-5.0–22.2
		weighted	5.0	0.6–10.6	0.3–15.2	7.0	0.7–15.8	-3.3–18.7
Northeast	277.5	unweighted	10.1	3.6–16.4	-3.9–18.8	15.7	10.5–24.5	5.9–32.7
		weighted	7.2	0.2–15.2	-3.9–17.1	12.9	1.0–23.4	0.4–30.3
Southeast	327.9	unweighted	6.3	-3.5–14.6	-8.5–18.0	7.7	-8.6–16.9	-18.7–28.1
		weighted	2.6	0.3–11.7	-7.8–17.7	1.3	-2.7–16.9	-18.7–26.2
N. Great Plains	133.7	unweighted	16.4	7.9–21.6	-2.0–36.7	26.1	12.8–37.7	-1.6–63.4
		weighted	14.5	1.4–19.5	0.7–36.7	19.0	2.5–35.1	1.1–63.4
S. Great Plains	210.2	unweighted	2.5	-4.0–9.6	-16.4–15.3	-0.6	-12.9–9.8	-16.7–14.6
		weighted	0.7	-3.2–6.0	-10.5–15.3	-0.1	-9.3–8.0	-13.8–14.6
Midwest	250.7	unweighted	12.3	6.6–18.4	1.5–21.1	20.5	11.7–30.7	7.2–36.7
		weighted	8.5	0.8–16.6	0.5–21.1	16.0	1.4–28.6	0.8–36.7
Northwest	170.4	unweighted	6.6	-3.0–12.8	-7.8–20.9	7.3	0.2–16.1	-8.4–24.5
		weighted	1.4	-1.8–11.0	-5.9–16.2	4.8	0.3–13.7	-3.4–24.5
Southwest	83.4	unweighted	-1.4	-12.5–9.5	-18.1–24.1	-10.8	-19.5–2.1	-23.6–11.6
		weighted	0.1	-9.1–6.4	-18.1–12.5	-2.8	-17.9–0.5	-22.3–9.0
Alaska	80.7	unweighted	15.9	7.2–28.4	2.4–34.8	38.6	23.0–53.9	9.3–70.9
		weighted	11.1	0.5–21.6	0.3–33.1	35.6	1.6–52.0	1.1–60.7
Hawaii	586.1	unweighted	-0.3	-18.1–13.5	-25.9–19.1	-4.2	-23.8–19.8	-34.7–32.7
		weighted	-0.5	-18.1–8.0	-25.9–18.9	-0.9	-21.3–8.9	-34.7–25.5

Table A9: Weighted and unweighted regional average summer precipitation change (Δ%)

JJA RCP 8.5			2040–2059 change (Δ%)			2080–2099 change (Δ%)		
Region	1981–2010 (mm)	Method	50	17–83	5–95	50	17–83	5–95
CONUS	212.5	unweighted	0.1	-6.5–5.8	-15.5–8.3	-0.3	-13.4–5.4	-22.1–9.9
		weighted	-0.2	-3.8–4.4	-8.4–7.8	-0.3	-8.3–3.3	-17.2–9.9
Northeast	309.5	unweighted	2.2	-2.3–8.8	-4.1–12.7	2.3	-4.7–18.7	-6.8–26.2
		weighted	0.3	-0.7–8.0	-3.0–12.7	0.3	-2.1–12.3	-5.8–26.2
Southeast	365.5	unweighted	2.6	-7.7–10.5	-14.2–19.1	-2.4	-14.5–12.4	-21.5–18.1
		weighted	0.2	-5.3–5.9	-14.2–11.9	-0.5	-13.7–11.5	-17.1–16.1
N. Great Plains	167.2	unweighted	-5.2	-13.4–4.2	-20.0–19.1	-10.8	-23.3–3.3	-36.0–12.3
		weighted	-0.5	-10.2–2.8	-19.7–8.5	-3.5	-22.2–2.2	-25.8–12.3
S. Great Plains	237.4	unweighted	-1.6	-8.9–6.0	-18.3–13.7	-7.0	-20.2–5.5	-23.5–13.2
		weighted	-0.1	-8.4–4.6	-16.8–9.0	-0.5	-18.4–1.5	-21.7–12.5
Midwest	304.2	unweighted	-3.2	-9.3–7.2	-17.1–12.9	-3.9	-16.8–7.6	-29.8–12.8
		weighted	-0.3	-6.7–6.5	-11.0–8.9	-0.2	-10.3–5.9	-21.4–11.8
Northwest	73.1	unweighted	-5.4	-22.5–7.5	-28.6–18.4	-15.6	-31.5–3.9	-55.8–29.0
		weighted	-1.1	-18.3–1.9	-24.6–8.4	-5.0	-29.4—0.3	-49.1–14.4
Southwest	78.3	unweighted	3.7	-8.9–15.9	-21.4–22.3	1.4	-20.8–23.3	-28.4–34.6
		weighted	0.9	-2.1–12.4	-16.7–19.0	1.0	-10.0–20.3	-26.9–31.5
Alaska	184.7	unweighted	14.8	9.0–20.8	4.4–25.8	28.9	18.2–40.6	12.2–64.0
		weighted	12.5	0.7–18.5	0.6–22.9	22.1	1.9–38.0	0.5–57.0
Hawaii	472.8	unweighted	-0.1	-14.1–18.3	-30.8–29.7	-3.6	-15.2–22.3	-37.6–49.0
		weighted	-0.2	-8.7–12.1	-30.8–22.2	-0.5	-12.8–17.4	-37.6–45.5

Table A10: Weighted and unweighted regional average autumn precipitation change (Δ%)

SON RCP 8.5			2040–2059 change (Δ%)			2080–2099 change (Δ%)		
Region	1981–2010 (mm)	Method	50	17–83	5–95	50	17–83	5–95
CONUS	182.0	unweighted	3.8	-0.4–8.7	-2.0–10.8	5.8	-1.9–10.9	-7.0–19.9
		weighted	2.2	-0.2–7.9	-2.0–10.2	3.3	-0.1–8.9	-7.0–18.8
Northeast	288.2	unweighted	3.9	-3.4–9.6	-5.4–13.7	6.9	-0.6–13.5	-9.0–15.9
		weighted	1.3	-0.2–6.5	-4.4–10.5	3.1	-0.2–12.0	-9.0–13.9
Southeast	306.0	unweighted	6.3	-1.7–16.5	-6.4–18.5	9.1	0.1–20.3	-15.6–27.7
		weighted	3.9	-0.0–12.6	-6.4–17.7	3.7	0.1–18.4	-15.6–26.6
N. Great Plains	93.1	unweighted	4.4	-3.4–11.8	-8.9–20.3	9.5	-3.1–15.6	-10.1–35.0
		weighted	0.9	-0.8–11.8	-8.8–20.3	2.0	-0.5–12.0	-8.9–23.9
S. Great Plains	201.9	unweighted	3.5	-7.9–11.0	-11.4–16.5	1.8	-15.6–13.0	-23.7–25.3
		weighted	-0.1	-7.0–8.9	-11.4–15.0	0.0	-15.6–5.7	-23.7–22.5
Midwest	233.4	unweighted	5.1	-1.2–9.3	-10.4–12.7	6.5	-1.5–12.7	-13.4–16.7
		weighted	2.2	-0.4–8.2	-4.5–12.7	3.5	-0.2–11.0	-13.4–16.0
Northwest	168.4	unweighted	2.3	-10.5–14.6	-12.1–16.7	9.2	-6.9–18.5	-12.9–27.6
		weighted	0.1	-7.4–13.8	-11.9–16.7	0.9	-3.9–15.7	-12.0–20.3
Southwest	80.3	unweighted	-1.6	-9.3–11.8	-22.4–19.6	-1.7	-9.6–13.8	-27.6–24.2
		weighted	-0.0	-6.3–7.5	-17.5–18.6	0.1	-8.9–11.6	-17.9–17.7
Alaska	170.1	unweighted	16.1	10.4–21.6	5.0–27.4	32.4	25.4–40.1	22.6–48.2
		weighted	11.7	0.7–18.5	0.2–26.5	31.2	1.4–36.8	0.9–41.3
Hawaii	627.7	unweighted	5.1	-8.2–21.0	-17.9–26.2	13.3	-2.5–43.8	-15.4–64.0
		weighted	1.0	-1.6–15.4	-17.9–26.2	5.1	-0.3–35.8	-15.4–44.3

Table A11: Weighted and unweighted projections of expected regional average (population-weighted) Category II+ ACP Humid Heat Stroke Index days per summer

RCP 8.5			2020–2039	2040–2059	2080–2099	2120–2139	2140–2159	2180–2199
Region	1981–2010	Method						
CONUS	4.65	weighted	10.21	17.21	34.93	49.88	54.42	60.01
		unweighted	10.36	16.83	33.59	49.1	53.83	59.73
Northeast	3.25	weighted	8.11	16.15	39.47	60.73	66.81	74.18
		unweighted	8.28	15.65	37.81	60.72	67.3	75.75
Southeast	8.24	weighted	18.52	30.49	56.73	74.05	78.68	83.36
		unweighted	18.82	29.87	55.63	74.4	79.43	84.45
N. Great Plains	1.45	weighted	3.16	5.58	14.28	25.25	30.09	36.79
		unweighted	3.18	5.41	12.91	22.63	27.27	33.98
S. Great Plains	8.85	weighted	14.9	19.92	30.06	38.54	41.42	45.33
		unweighted	14.91	19.63	29.23	37.03	39.69	43.38
Midwest	4.82	weighted	11.37	19.96	42.81	62.77	68.37	75.27
		unweighted	11.57	19.53	40.69	61.94	68.26	76
Northwest	0.16	weighted	0.52	1.48	9.66	23.68	30.27	39.17
		unweighted	0.5	1.36	7.5	20.13	26.96	36.9
Southwest	0.05	weighted	0.11	0.26	1.5	4.78	6.75	10.3
		unweighted	0.1	0.23	0.96	2.83	4.05	6.53
Alaska	0	weighted	0	0	0.18	3.92	7.77	15.36
		unweighted	0	0	0.06	1.39	3.17	8.44
Hawaii	1.63	weighted	6.76	16.89	48.26	67.16	70.95	75.92
		unweighted	7.16	16.14	47.14	68.53	72.88	77.12

Table A12: Weighted and unweighted projections of expected regional average (population-weighted) Category III+ ACP Humid Heat Stroke Index days per summer

RCP 8.5			2020–2039	2040–2059	2080–2099	2120–2139	2140–2159	2180–2199
Region	1981–2010	Method						
CONUS	0.03	weighted	0.17	0.75	7.49	21.82	28.22	37.15
		unweighted	0.17	0.65	5.35	18.04	24.8	35.13
Northeast	0.05	weighted	0.22	1.03	9.82	29.47	38.1	49.93
		unweighted	0.23	0.87	7.12	25.25	34.53	48.68
Southeast	0.01	weighted	0.08	0.48	8.8	28.22	36.92	49.49
		unweighted	0.09	0.4	5.57	22.64	32.19	47.38
N. Great Plains	0.02	weighted	0.1	0.33	2.99	10.08	14.05	20.22
		unweighted	0.1	0.3	2.09	7.16	10.6	16.34
S. Great Plains	0.01	weighted	0.04	0.15	2.48	9.22	12.43	17.29
		unweighted	0.04	0.12	1.37	6.55	9.74	15.04
Midwest	0.08	weighted	0.49	1.95	14.23	34.62	42.87	53.54
		unweighted	0.49	1.73	11.31	30.34	39.48	51.91
Northwest	0	weighted	0.01	0.07	1.73	9.3	14.56	22.52
		unweighted	0.01	0.06	0.88	5.43	9.74	17.61
Southwest	0	weighted	0.01	0.02	0.18	1.35	2.27	3.82
		unweighted	0.01	0.02	0.07	0.37	0.71	1.54
Alaska	0	weighted	0	0	0	1.38	2.55	5.93
		unweighted	0	0	0	0.09	0.3	1.39
Hawaii	0	weighted	0	0.01	3.1	18.73	27.22	36.62
		unweighted	0	0.01	1.02	11.94	20.94	33.12

Table A13: Weighted and unweighted projections of expected regional average (population-weighted) Category IV ACP Humid Heat Stroke Index days per summer

RCP 8.5			2020–2039	2040–2059	2080–2099	2120–2139	2140–2159	2180–2199
Region	1981–2010	Method						
CONUS	0	weighted	0	0.01	0.79	6.27	10.23	17.13
		unweighted	0	0.01	0.29	2.79	5.47	11.54
Northeast	0	weighted	0	0.01	1.14	9	14.87	24.92
		unweighted	0	0.01	0.36	3.93	8.24	18.23
Southeast	0	weighted	0	0	0.36	5.54	9.88	18.26
		unweighted	0	0	0.08	1.54	3.67	9.75
N. Great Plains	0	weighted	0	0	0.24	2.82	4.89	8.89
		unweighted	0	0	0.07	0.9	2	4.76
S. Great Plains	0	weighted	0	0	0.05	1.17	2.11	4.15
		unweighted	0	0	0.01	0.14	0.38	1.25
Midwest	0	weighted	0	0.02	2.22	13.35	20.07	30.47
		unweighted	0	0.02	0.96	7.65	13.41	24.2
Northwest	0	weighted	0	0	0.18	2.9	5.51	11.29
		unweighted	0	0	0.05	0.71	1.94	5.75
Southwest	0	weighted	0	0	0.02	0.41	0.83	1.58
		unweighted	0	0	0.01	0.04	0.09	0.27
Alaska	0	weighted	0	0	0	0.73	1.51	2.3
		unweighted	0	0	0	0	0.01	0.1
Hawaii	0	weighted	0	0	0.01	2.43	4.99	12.03
		unweighted	0	0	0	0.08	0.42	3.92

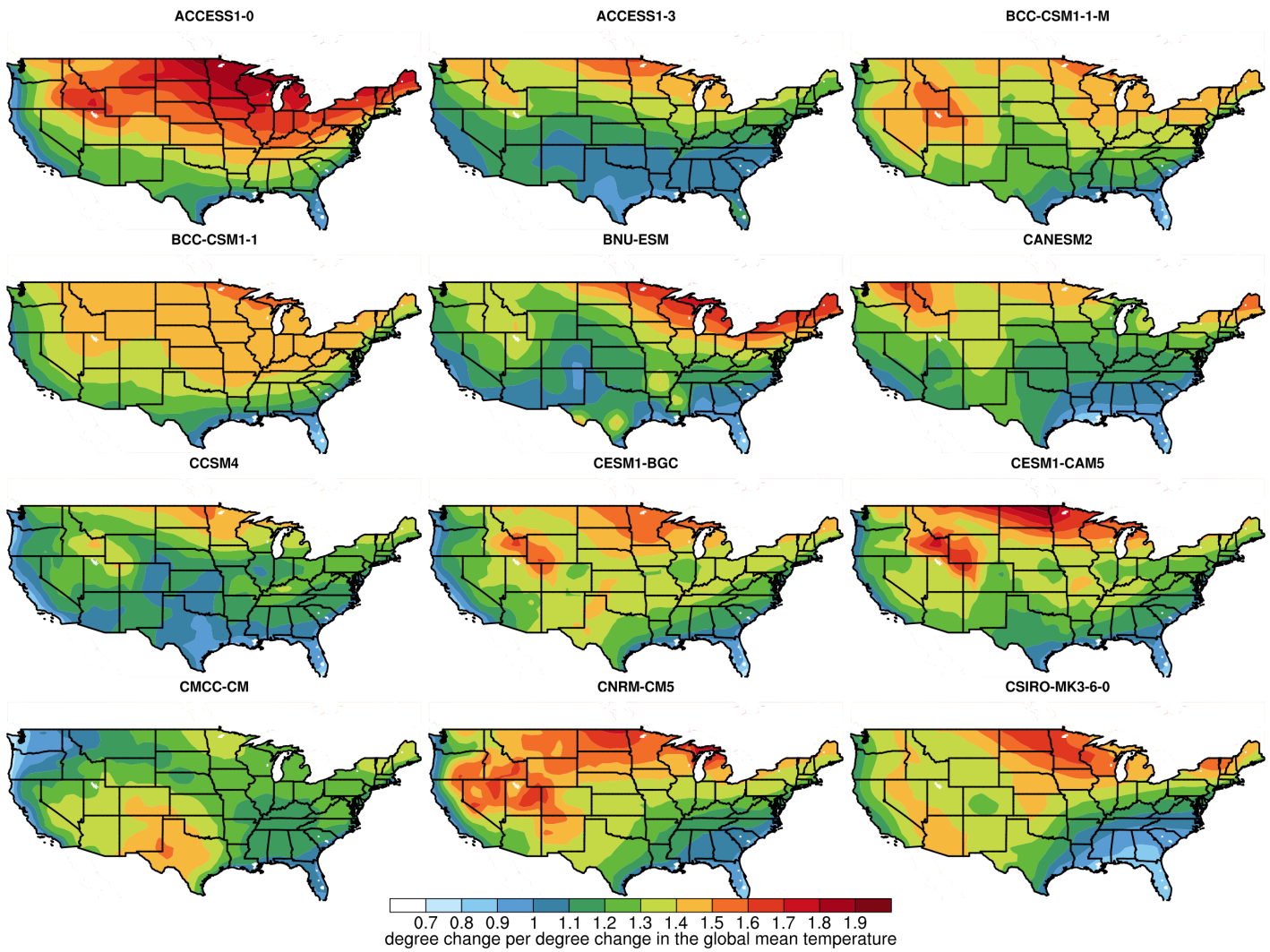

Figure A6: Annual surface temperature patterns for each CMIP5 model for RCP 8.5.

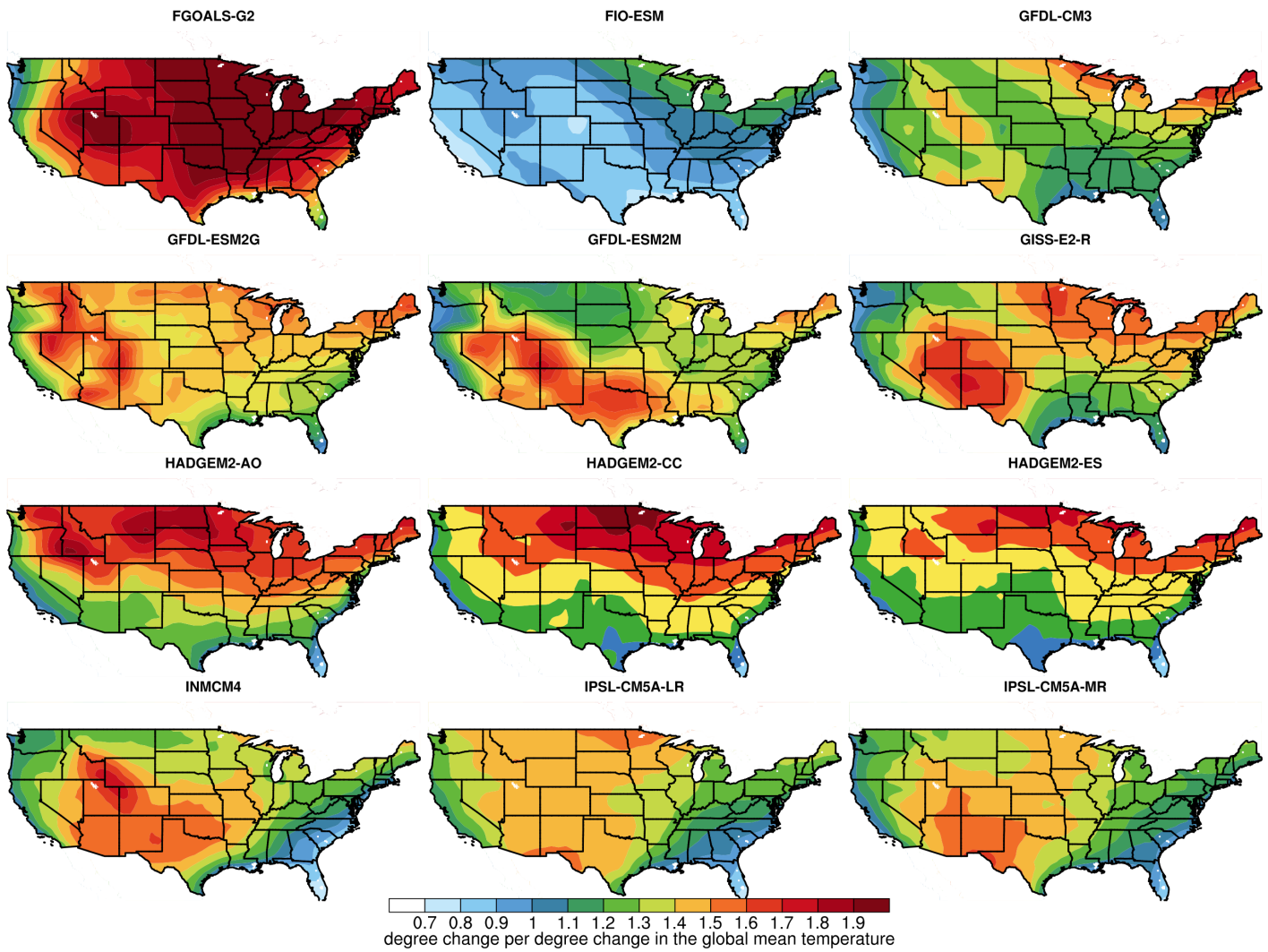

Figure A6: (con't)

Figure A6: (con't)

Figure A7: Annual daily precipitation rate patterns for each CMIP5 model.

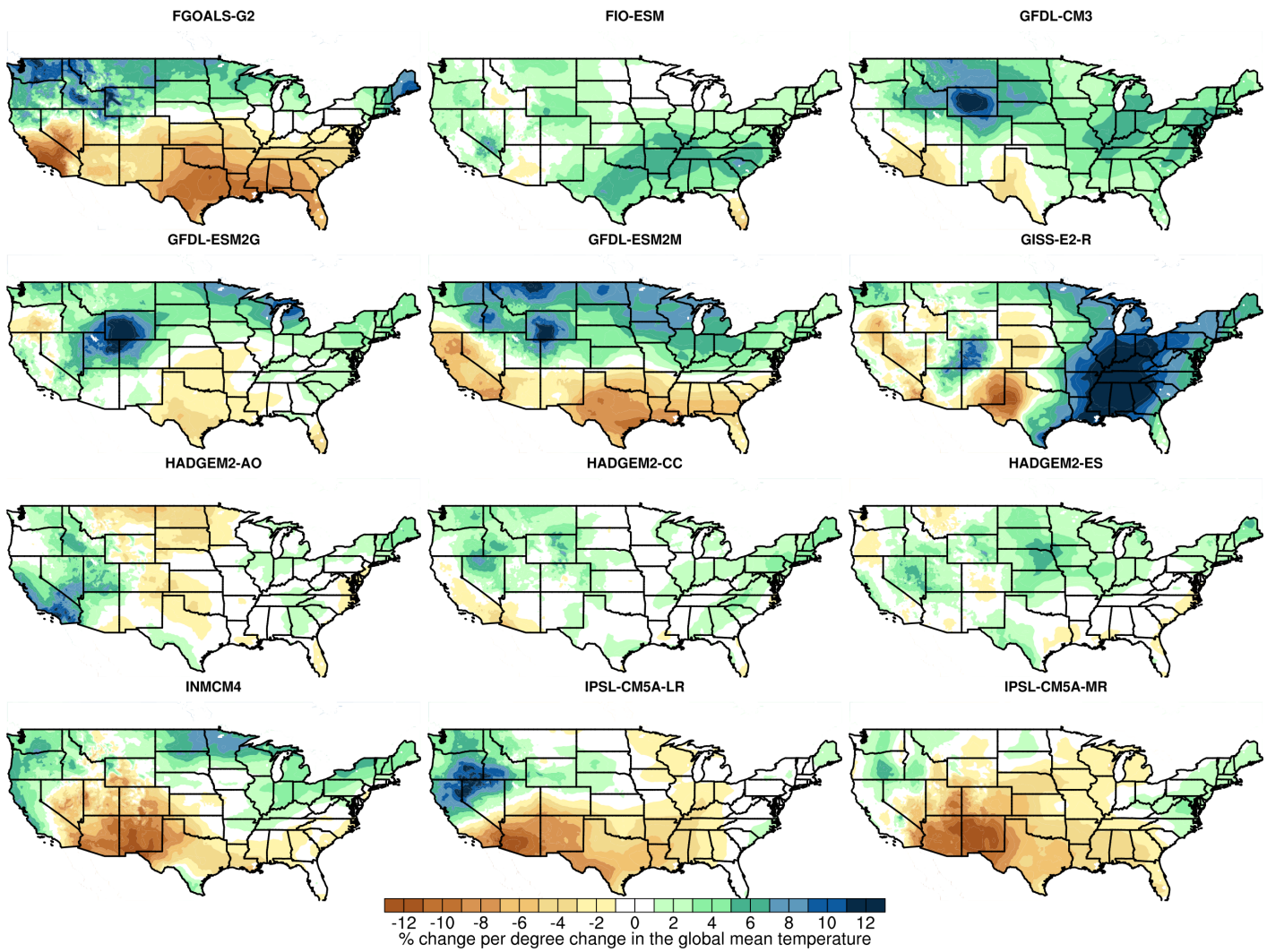

Figure A7: (con't)

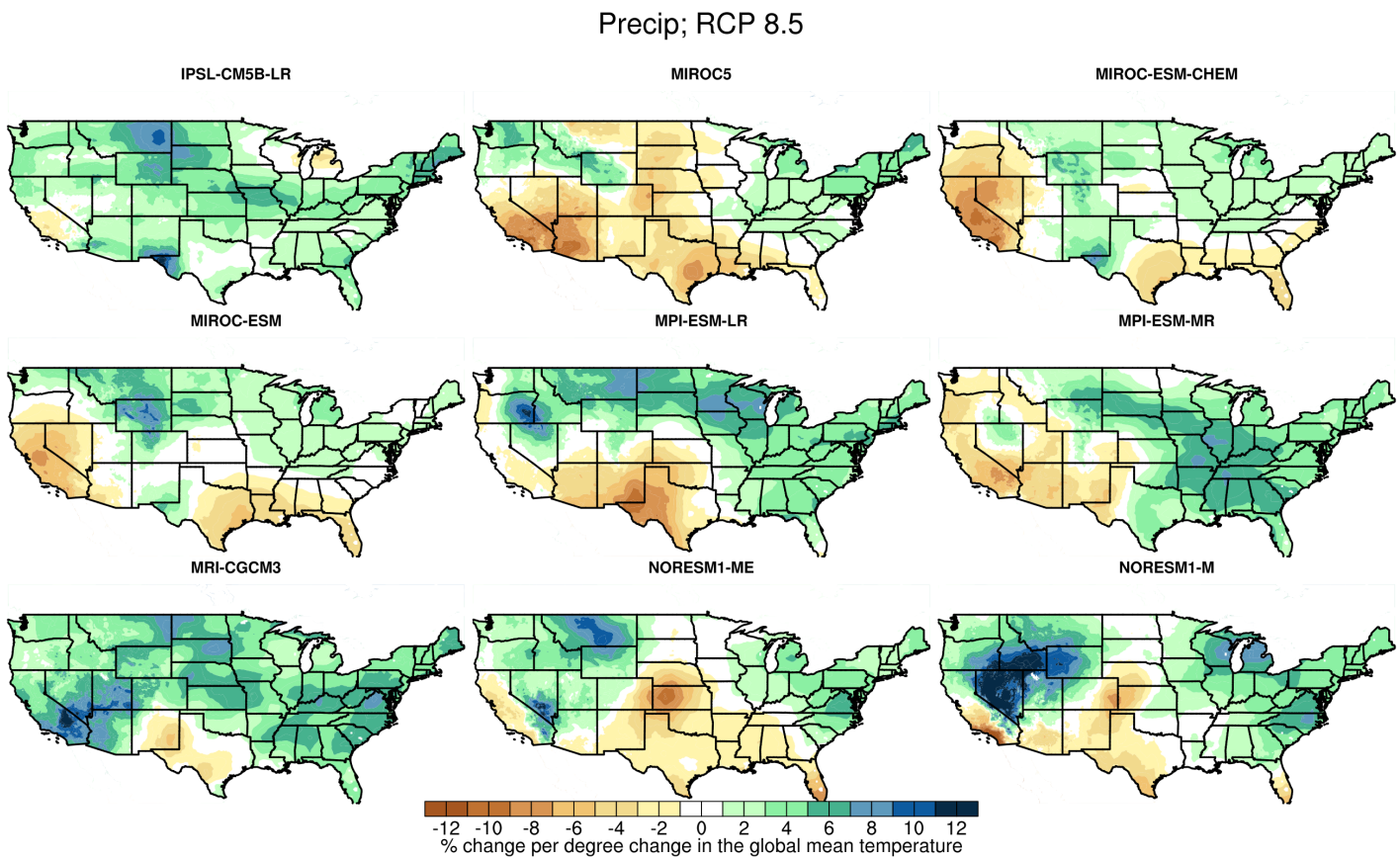

Figure A7: (con't)

A.2. Sea-level rise projections

The sea-level rise projections used in this analysis are described in depth in *Kopp et al.* (2014). We briefly summarize key elements of the methodology.

At a globally-averaged scale, sea-level change is driven primarily by changes in the amount of heat stored in the ocean (thermal expansion) and the amount of ice stored in glaciers and ice sheets. Smaller contributions to sea-level change are made by human-induced changes in the amount of water stored on land, through groundwater extraction and dam construction.

For impact analysis, it is important to estimate not just global mean sea-level (GMSL) change but also local sea-level change, as the impacts are experienced at particularly localities, not the global mean. Local sea-level (LSL) change differs from GMSL change due to numerous effects, including:

- ocean dynamics and 'steric' variations in the temperature and salinity of the ocean,
- changes in Earth's gravitational field and rotation and flexure of the Earth's lithosphere due to the redistribution of mass between land ice and the ocean (known as static-equilibrium effects),
- land motion and other effects associated with the ongoing response to the redistribution of mass since the end of the last ice age (known as glacial isostatic adjustment, GIA), and
- non-climatic effects, such as tectonics and sediment compaction due to both natural processes and fluid (groundwater or hydrocarbon) withdrawal.

Figure A8 summarizes the process used in constructing the sea-level rise projections for each RCP.

Projected sea-level rise due to thermal expansion, ocean dynamics, and steric effects (known here collectively as oceanographic effects) is based upon the projections of the CMIP5 models. One realization was used from each available model (Table A14), and each model was treated as an equally likely sample from an underlying normal distribution. Changes in the mass balance of glaciers were also indirectly based upon the CMIP5 models, via the surface mass balance model of *Marzeion et al.* (2012). The projections of *Marzeion et al.* (2012) for each CMIP5 model were similarly treated as equally likely samples from an underlying normal distributions.

Projections of changes in the Greenland and Antarctic ice sheets were assumed to follow log-normal distributions, with likely (17th to 83rd percentile) ranges from IPCC AR5 (*Church et al.*, 2013). As AR5 does not provide estimates beyond the 17th–83rd percentiles, the ratio of the 95th-to-83rd and 5th-to-17th percentiles from the expert elicitation study of *Bamber and Aspinall* (2013) were used to set the shape of the tail projections.

Estimates of GMSL change due to human-caused changes in land water storage are based on models of the relationship between total global population, impoundment of water in dams, and groundwater depletion (*Chao et al.*, 2008; *Wada et al.*, 2012; *Konikow*, 2011).

Background rates of GIA and non-climatic process were estimated from tide-gauge data using a Gaussian process model similar to that employed by *Kopp* (2013). Note that this approach assumes that background rates of sea-level change will continue unchanged; to the extent that these result from human activities, such as hydrocarbon extraction in western Gulf states, economic and policy changes can decrease or increase these rates in a fashion for which our projections do not account.

We combine probability distributions for the different components contributing to sea-level rise to construct sea-level rise projections for RCP 8.5, RCP 4.5, and RCP 2.6. We do not construct projections for RCP 6.0, as sea-level rise in RCP 4.5 and RCP 6.0 are indistinguishable in the 21st century (*Church et al.*, 2013), and insufficient model output is available to extend RCP 6.0 projections for oceanographic and glacial beyond 2100.

Our local sea-level rise projections (Table A15) can be compared with those of other sources. For example, under RCP 8.5, we project that sea-level at New York City will *likely* rise over the 21st century by between 0.7 and 1.3 m (2.1–4.2 ft), and *very likely* rise between 0.4 and 1.5 m (1.4–5.1 ft). By comparison, *Miller et al.* (2013)'s 'low' projection is 70 cm (comparable to our 17th percentile for RCP 8.5), their 'central' projection is 1.0 m (comparable to our 50th percentile), their 'high' projection is 1.4 cm (comparable to our 90th percentile), and their 'higher' projection is 1.6 m (comparable to our 97th percentile). We project a

1-in-200 probability that New York City will experience more than 2.1 m (6.9 ft) of sea-level rise, and a 1-in-1000 probability it will experience more than 3.1 m (9.9 ft).

Our 1-in-1000 probability GMSL projection for RCP 8.5, 2.5 m (8 ft) in 2100, is similar to other estimates of the maximum sea-level rise physically possible in the current century (e.g., *Miller et al.*, 2013; *Church et al.*, 2013). Accordingly, we interpret 1-in-1000 probability projections as the maximum physically plausible. Such high sea-level rise requires a fairly rapid collapse of the West Antarctic Ice Sheet (WAIS) (*Little et al.*, 2013) following its destabilization by effects such as grounding line retreat feedbacks (*Schoof*, 2007; *Gomez et al.*, 2012, 2013) or ice-cliff collapse feedbacks (*Bassis and Walker*, 2012; *Pollard and DeConto*, 2013). Observations indicate that WAIS may already have been destabilized (*Rignot et al.*, 2014; *Joughin et al.*, 2014), but do not yet suggest that the ensuing collapse will occur at the rates needed to reach the maximum-plausible 21st century sea-level rise. Other users may have alternative assessments of the likely rate of collapse, which may render high-end outcomes more likely than we estimate.

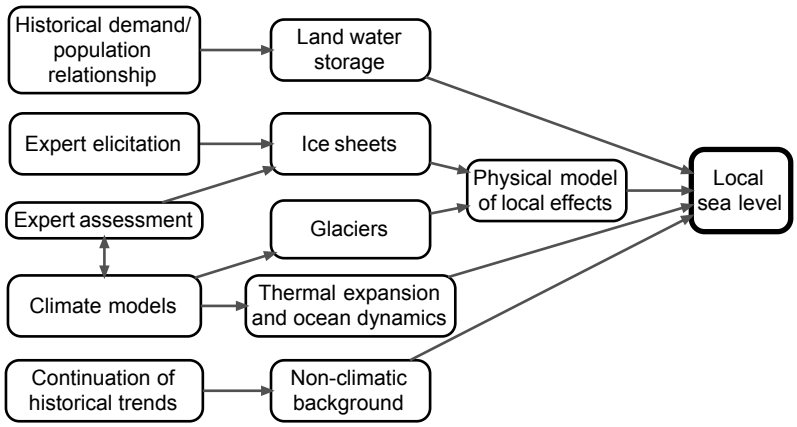

Figure A8: Flow of sea-level rise projection construction.

Bibliography

Arguez, A., I. Durre, S. Applequist, R. S. Vose, M. F. Squires, X. Yin, R. R. Heim Jr, and T. W. Owen (2012), NOAA's 1981-2010 US climate normals: An overview, *Bulletin of the American Meteorological Society*, *93*(11), 1687–1697, doi:10.1175/BAMS-D-11-00197.1.

Bamber, J. L., and W. P. Aspinall (2013), An expert judgement assessment of future sea level rise from the ice sheets, *Nature Climate Change*, *3*, 424–427, doi:10.1038/nclimate1778.

Bassis, J. N., and C. C. Walker (2012), Upper and lower limits on the stability of calving glaciers from the yield strength envelope of ice, *Proceedings of the Royal Society A: Mathematical, Physical and Engineering Science*, *468*(2140), 913–931, doi:10.1098/rspa.2011.0422.

Brekke, L., B. L. Thrasher, E. P. Maurer, , and T. Pruitt (2013), *Downscaled CMIP3 and CMIP5 Climate Projections: Release of Downscaled CMIP5 Climate Projections, Comparison with Preceding Information, and Summary of User Needs*, 116 pp., U.S. Department of the Interior, Bureau of Reclamation, Technical Service Center, Denver, Colorado.

Chao, B. F., Y. H. Wu, and Y. S. Li (2008), Impact of artificial reservoir water impoundment on global sea level, *Science*, *320*(5873), 212–214, doi:10.1126/science.1154580.

Church, J. A., P. U. Clark, et al. (2013), Chapter 13: Sea level change, in *Climate Change 2013: the Physical Science Basis*, edited by T. F. Stocker, D. Qin, G.-K. Plattner, M. Tignor, S. K. Allen, J. Boschung, A. Nauels, Y. Xia, V. Bex, and P. Midgley, Cambridge University Press.

Table A14: CMIP5 models used for sea-level projections

Model	Oceanographic effects			Glaciers		
	RCP 8.5	RCP 4.5	RCP 2.6	RCP 8.5	RCP 4.5	RCP 2.6
access1-0	1	1				
access1-3	1	1				
bcc-csm1-1	2	2	2	2	2	2
bcc-csm1-1-m	1	1	1			
canesm2	1	2	2	1	2	2
ccsm4	1	1	1	1	1	1
cmcc-cesm	1					
cmcc-cm	1	1				
cmcc-cms	1	1				
cnrm-cm5	2	2	1	2	2	1
csiro-mk3-6-0	1	1	1	2	2	1
gfdl-cm3	1	2	1	1	1	1
gfdl-esm2g	1	1	1			
gfdl-esm2m	1	1	1			
giss-e2-r	2	2	2	2	2	
giss-e2-r-cc	1	1				
hadgem2-cc	1					
hadgem2-es	1		2	2	2	2
inmcm4	1	1		1	1	
ipsl-cm5a-lr	2	2	2	2	2	2
ipsl-cm5a-mr	1	2	1			
miroc-esm	1	2	1	1	1	1
miroc-esm-chem	1	1	1			
miroc5	1			1	1	1
mpi-esm-lr	2	2	2	2	2	2
mpi-esm-mr	1	1	1			
mri-cgcm3	1		1	1	1	1
noresm1-m	1	2	1	1	2	1
noresm1-me	1	1	1			

1 = to 2100, 2 = to 2200.

Table A15: Sea-level rise projections

Feet above 2000	RCP 8.5				RCP 4.5				RCP 2.6			
	Likely	90% range	99% range	1-in-1000	*Likely*	90% range	99% range	1-in-1000	*Likely*	90% range	99% range	1-in-1000
GLOBAL												
2030	0.4–0.5	0.3–0.6	0.3–0.7	0.8	0.4–0.5	0.3–0.6	0.3–0.7	0.7	0.4–0.5	0.3–0.6	0.3–0.7	0.7
2050	0.8–1.1	0.7–1.3	0.5–1.6	2.0	0.7–1.0	0.6–1.1	0.5–1.4	1.9	0.7–0.9	0.6–1.1	0.5–1.4	1.8
2100	2.0–3.3	1.7–4.0	1.3–5.8	8.1	1.5–2.5	1.2–3.1	0.8–4.8	7.1	1.2–2.1	0.9–2.7	0.6–4.6	6.9
2150	3.2–5.9	2.6–7.6	1.8–12.1	17.8	2.0–4.3	1.4–5.7	0.7–10.0	15.6	1.5–3.5	1.1–4.9	0.7–9.6	15
2200	4.4–9.2	3.2–12.3	2.0–20.7	31.1	2.4–6.4	1.3–8.9	0.2–16.9	27.3	1.7–5.3	0.9–7.8	0.2–16.4	26.5
PORTLAND, ME												
2030	0.4–0.8	0.2–0.9	0.0–1.2	1.3	0.4–0.7	0.2–0.8	0.1–1.0	1.1	0.3–0.8	0.2–0.9	0.0–1.1	1.3
2050	0.7–1.4	0.4–1.7	0.1–2.2	2.5	0.6–1.3	0.4–1.5	0.1–2.0	2.3	0.5–1.3	0.3–1.6	-0.1–2.1	2.4
2100	1.7–3.8	1.0–4.6	0.1–6.6	9.4	1.3–2.9	0.7–3.6	0.0–5.5	7.9	0.9–2.4	0.4–3.1	-0.3–5.2	7.6
2150	3.1–5.7	2.4–7.2	1.5–12.9	18.7	1.7–4.4	0.8–5.9	-0.3–11.2	16.5	1.3–3.3	0.8–4.9	0.3–10.5	16.4
2200	4.0–8.3	2.9–11.1	1.6–21.4	32.1	1.8–6.2	0.6–8.9	-0.9–18.8	28.4	1.1–4.8	0.5–7.8	-0.3–18.2	28.4
BOSTON, MA												
2030	0.4–0.9	0.3–1.0	0.1–1.2	1.4	0.4–0.8	0.3–0.9	0.1–1.1	1.2	0.4–0.8	0.3–1.0	0.0–1.2	1.3
2050	0.8–1.6	0.6–1.8	0.2–2.3	2.6	0.8–1.4	0.5–1.7	0.2–2.1	2.4	0.7–1.4	0.4–1.7	0.0–2.2	2.6
2100	2.0–4.0	1.3–4.9	0.4–6.8	9.7	1.5–3.1	1.0–3.8	0.3–5.8	8.2	1.2–2.6	0.7–3.3	0.0–5.4	7.9
2150	3.5–6.1	2.8–7.6	2.0–13.3	19.3	2.1–4.8	1.2–6.3	0.1–11.7	17	1.6–3.7	1.2–5.3	0.7–10.9	16.8
2200	4.5–8.9	3.5–11.8	2.2–22.2	33	2.4–6.7	1.1–9.5	-0.4–19.4	29	1.7–5.4	1.0–8.3	0.3–18.8	29.0
NEWPORT, RI												
2030	0.4–0.9	0.3–1.1	0.0–1.3	1.5	0.5–0.8	0.4–0.9	0.2–1.1	1.2	0.4–0.8	0.3–1.0	0.1–1.2	1.3
2050	0.9–1.6	0.6–1.9	0.3–2.3	2.6	0.8–1.5	0.6–1.7	0.3–2.1	2.4	0.7–1.4	0.5–1.7	0.1–2.2	2.5
2100	2.1–4.1	1.4–5.0	0.5–6.9	9.9	1.6–3.2	1.1–3.9	0.3–5.9	8.3	1.2–2.7	0.8–3.4	0.1–5.5	8.0
2150	3.7–6.3	3.0–7.8	2.0–13.6	19.7	2.2–5.0	1.3–6.5	0.2–11.9	17.2	1.8–3.9	1.3–5.5	0.7–11.1	17.1
2200	4.7–9.2	3.6–12.1	2.3–22.5	33.6	2.5–7.0	1.3–9.7	-0.3–19.7	29.4	1.8–5.6	1.1–8.5	0.4–19.1	29.3
NEW YORK, NY												
2030	0.4–1.0	0.2–1.2	0.0–1.4	1.6	0.5–0.8	0.4–1.0	0.2–1.1	1.2	0.4–0.9	0.3–1.0	0.1–1.2	1.4
2050	0.9–1.6	0.6–1.9	0.3–2.4	2.7	0.9–1.5	0.6–1.7	0.3–2.2	2.5	0.8–1.5	0.5–1.7	0.2–2.2	2.5
2100	2.1–4.2	1.4–5.1	0.5–6.9	9.9	1.7–3.3	1.1–4.0	0.4–6.0	8.3	1.3–2.8	0.9–3.5	0.2–5.6	8.0
2150	3.7–6.5	2.9–8.0	1.8–13.7	20	2.3–5.1	1.4–6.7	0.3–11.9	17.1	1.9–4.0	1.4–5.6	0.8–11.1	16.9
2200	4.9–9.5	3.8–12.3	2.3–22.6	33.6	2.7–7.2	1.5–9.9	-0.1–19.7	29.4	2.0–5.7	1.3–8.7	0.6–19.0	29.1
ATLANTIC CITY, NJ												
2030	0.6–1.0	0.4–1.1	0.2–1.3	1.5	0.6–0.9	0.5–1.0	0.3–1.2	1.3	0.5–1.0	0.4–1.1	0.2–1.3	1.5
2050	1.0–1.8	0.8–2.0	0.4–2.5	2.8	1.0–1.6	0.8–1.9	0.5–2.3	2.6	0.9–1.6	0.7–1.9	0.3–2.4	2.7
2100	2.4–4.5	1.7–5.3	0.8–7.2	10.3	2.0–3.6	1.4–4.3	0.7–6.3	8.7	1.7–3.1	1.2–3.8	0.5–6.0	8.3
2150	4.2–6.9	3.4–8.4	2.5–14.1	20.6	2.8–5.6	1.9–7.2	0.7–12.5	17.8	2.4–4.5	1.9–6.1	1.3–11.7	17.5
2200	5.5–10.0	4.4–13.0	3.0–23.4	34.4	3.3–7.9	2.1–10.6	0.4–20.5	30.4	2.7–6.4	2.0–9.4	1.2–19.8	30
PHILADELPHIA, PA												
2030	0.4–0.9	0.3–1.1	0.1–1.3	1.4	0.5–0.8	0.4–0.9	0.2–1.1	1.2	0.4–0.9	0.3–1.0	0.1–1.3	1.4
2050	0.9–1.6	0.6–1.9	0.3–2.3	2.6	0.8–1.5	0.6–1.7	0.3–2.1	2.4	0.8–1.5	0.5–1.7	0.2–2.2	2.5
2100	2.1–4.1	1.4–5.0	0.5–6.8	9.8	1.7–3.3	1.1–4.0	0.4–5.9	8.3	1.3–2.8	0.9–3.5	0.2–5.6	7.9
2150	3.7–6.3	2.9–7.9	2.0–13.5	19.9	2.3–5.1	1.4–6.6	0.3–11.7	17	1.9–4.0	1.4–5.5	0.8–11.1	16.8
2200	4.9–9.3	3.8–12.2	2.4–22.5	33.4	2.7–7.1	1.5–9.8	0.0–19.5	29.3	2.0–5.7	1.3–8.7	0.6–18.9	29
LEWES, DE												
2030	0.5–0.9	0.4–1.1	0.2–1.3	1.4	0.5–0.8	0.4–1.0	0.3–1.1	1.2	0.5–0.9	0.4–1.0	0.2–1.2	1.3
2050	1.0–1.7	0.7–1.9	0.4–2.4	2.7	0.9–1.5	0.7–1.7	0.5–2.2	2.5	0.9–1.5	0.7–1.7	0.4–2.1	2.6
2100	2.3–4.2	1.7–5.0	0.8–7.0	9.9	1.9–3.4	1.4–4.1	0.7–6.0	8.4	1.5–2.9	1.1–3.6	0.5–5.8	8.1
2150	3.9–6.7	3.2–8.2	2.2–13.8	20.4	2.6–5.3	1.8–6.7	0.8–12.1	17.5	2.1–4.3	1.7–5.8	1.1–11.4	17.2
2200	5.2–9.8	4.2–12.7	2.8–23.0	34.1	3.1–7.4	1.9–10.1	0.5–20.0	30	2.4–6.1	1.7–9.1	0.9–19.4	29.6
BALTIMORE, MD												
2030	0.5–0.9	0.3–1.0	0.1–1.2	1.3	0.5–0.8	0.4–0.9	0.2–1.1	1.2	0.5–0.8	0.3–1.0	0.1–1.2	1.3
2050	0.9–1.6	0.7–1.8	0.4–2.3	2.6	0.9–1.5	0.7–1.7	0.4–2.1	2.5	0.8–1.4	0.6–1.7	0.3–2.1	2.5
2100	2.2–4.1	1.6–4.9	0.7–6.8	9.7	1.7–3.2	1.3–3.9	0.6–5.9	8.2	1.4–2.8	1.0–3.5	0.4–5.6	7.9
2150	3.7–6.4	3.0–7.9	2.1–13.4	19.9	2.4–5.0	1.6–6.5	0.6–11.8	17.1	2.0–4.1	1.5–5.6	1.0–11.1	16.8
2200	5.0–9.4	3.9–12.3	2.6–22.5	33.4	2.9–7.1	1.7–9.8	0.3–19.5	29.3	2.2–5.8	1.5–8.8	0.7–19.0	29
WASHINGTON, DC												
2030	0.5–0.9	0.4–1.0	0.2–1.2	1.3	0.5–0.8	0.4–0.9	0.2–1.1	1.2	0.5–0.8	0.3–1.0	0.2–1.2	1.3
2050	0.9–1.5	0.7–1.8	0.4–2.2	2.6	0.9–1.4	0.7–1.6	0.4–2.0	2.4	0.8–1.4	0.6–1.6	0.3–2.0	2.5
2100	2.2–4.0	1.6–4.8	0.7–6.7	9.6	1.7–3.2	1.2–3.9	0.6–5.8	8.1	1.4–2.8	1.0–3.4	0.4–5.6	7.9
2150	3.7–6.3	3.0–7.9	2.1–13.4	19.8	2.4–5.0	1.6–6.5	0.6–11.7	17	2.0–4.0	1.5–5.6	1.0–11.1	16.8
2200	5.0–9.4	3.9–12.2	2.6–22.4	33.3	2.8–7.1	1.7–9.7	0.3–19.4	29.3	2.1–5.8	1.4–8.7	0.7–18.9	28.9

Table A15: Sea-level rise projections (con't)

Feet above 2000	RCP 8.5				RCP 4.5				RCP 2.6			
	Likely	90% range	99% range	1-in-1000	*Likely*	90% range	99% range	1-in-1000	*Likely*	90% range	99% range	1-in-1000
NORFOLK, VA												
2030	0.6–1.0	0.5–1.1	0.3–1.3	1.4	0.6–0.9	0.5–1.0	0.3–1.2	1.3	0.6–0.9	0.5–1.1	0.3–1.2	1.3
2050	1.1–1.7	0.9–2.0	0.6–2.4	2.8	1.1–1.6	0.9–1.8	0.6–2.2	2.6	1.0–1.6	0.8–1.8	0.5–2.2	2.7
2100	2.5–4.4	1.9–5.2	1.1–7.2	10.1	2.1–3.6	1.6–4.2	1.0–6.2	8.5	1.8–3.1	1.4–3.8	0.8–6.0	8.4
2150	4.3–7.0	3.5–8.6	2.6–14.1	20.6	3.0–5.6	2.2–7.1	1.2–12.4	17.9	2.5–4.6	2.1–6.2	1.5–11.8	17.6
2200	5.7–10.3	4.7–13.2	3.4–23.4	34.6	3.6–7.9	2.5–10.5	1.0–20.3	30.6	2.9–6.7	2.2–9.6	1.4–20.0	30.1
WILMINGTON, NC												
2030	0.4–0.7	0.3–0.9	0.1–1.1	1.2	0.4–0.7	0.3–0.8	0.2–1.0	1	0.4–0.7	0.3–0.8	0.1–1.0	1.1
2050	0.8–1.4	0.6–1.6	0.3–2.0	2.4	0.7–1.2	0.5–1.4	0.3–1.8	2.3	0.7–1.2	0.5–1.4	0.3–1.8	2.3
2100	1.9–3.6	1.4–4.3	0.7–6.4	9.2	1.5–2.8	1.1–3.4	0.5–5.6	7.9	1.2–2.4	0.8–3.1	0.3–5.3	7.8
2150	3.3–5.9	2.7–7.5	1.9–13.0	19.5	2.0–4.5	1.3–6.0	0.5–11.3	17	1.6–3.7	1.1–5.3	0.5–11.0	16.8
2200	4.5–8.9	3.5–11.9	2.4–22.2	33.3	2.3–6.5	1.3–9.3	0.0–19.1	29.5	1.6–5.5	0.9–8.4	0.1–18.9	29
CHARLESTON, SC												
2030	0.5–0.8	0.3–0.9	0.2–1.1	1.2	0.5–0.8	0.4–0.9	0.2–1.0	1.1	0.5–0.8	0.4–0.9	0.2–1.0	1.1
2050	0.9–1.4	0.7–1.6	0.5–2.0	2.6	0.8–1.3	0.7–1.5	0.5–1.9	2.3	0.8–1.3	0.7–1.5	0.5–1.8	2.3
2100	2.1–3.8	1.6–4.5	0.9–6.6	9.4	1.7–3.0	1.3–3.6	0.8–5.8	8.1	1.4–2.6	1.0–3.3	0.5–5.6	7.9
2150	3.6–6.2	3.0–7.9	2.2–13.2	19.8	2.4–4.9	1.7–6.3	0.8–11.6	17.3	1.9–4.0	1.5–5.6	0.9–11.2	17
2200	4.8–9.4	3.9–12.4	2.9–22.5	33.6	2.8–7.0	1.8–9.7	0.4–19.5	30.1	2.1–5.9	1.4–8.9	0.6–19.2	29.5
FORT PULASKI, GA												
2030	0.5–0.8	0.3–0.9	0.2–1.1	1.2	0.5–0.8	0.4–0.9	0.2–1.0	1.1	0.5–0.8	0.4–0.9	0.2–1.0	1.1
2050	0.9–1.4	0.7–1.7	0.5–2.0	2.6	0.9–1.3	0.7–1.5	0.5–1.9	2.3	0.8–1.3	0.7–1.5	0.5–1.8	2.3
2100	2.2–3.8	1.7–4.6	0.9–6.6	9.4	1.7–3.0	1.3–3.7	0.8–5.8	8.1	1.4–2.7	1.1–3.3	0.6–5.6	7.9
2150	3.7–6.3	3.1–8.0	2.3–13.3	19.8	2.4–4.9	1.7–6.4	0.8–11.6	17.4	2.0–4.1	1.5–5.7	1.0–11.2	17
2200	5.0–9.5	4.0–12.5	3.0–22.7	33.8	2.9–7.1	1.8–9.8	0.5–19.5	30.2	2.2–6.0	1.4–8.9	0.7–19.2	29.5
MIAMI, FL												
2030	0.4–0.7	0.3–0.9	0.1–1.1	1.2	0.4–0.7	0.3–0.8	0.1–1.0	1.1	0.4–0.7	0.3–0.8	0.2–0.9	1.0
2050	0.8–1.3	0.6–1.5	0.4–1.9	2.5	0.7–1.2	0.6–1.4	0.4–1.7	2.2	0.7–1.1	0.6–1.3	0.4–1.7	2.2
2100	2.0–3.6	1.5–4.3	0.9–6.4	9.3	1.5–2.8	1.1–3.4	0.6–5.6	8.1	1.2–2.4	0.9–3.0	0.5–5.4	7.9
2150	3.3–6.2	2.6–7.9	1.6–13.3	20.1	2.1–4.6	1.3–6.1	0.4–11.5	17.6	1.6–3.8	1.1–5.4	0.6–11.0	17.2
2200	4.5–9.4	3.3–12.6	2.1–22.5	34.4	2.4–6.8	1.3–9.6	-0.1–19.3	30.7	1.7–5.7	0.9–8.6	0.1–19.0	30.1
PENSACOLA, FL												
2030	0.4–0.7	0.3–0.8	0.1–0.9	1.0	0.4–0.6	0.3–0.8	0.1–0.9	1	0.4–0.7	0.2–0.8	0.1–1.0	1.1
2050	0.8–1.3	0.6–1.5	0.4–1.8	2.4	0.7–1.1	0.6–1.3	0.3–1.6	2.1	0.7–1.1	0.5–1.3	0.3–1.7	2.2
2100	1.8–3.5	1.3–4.2	0.7–6.2	9.1	1.4–2.7	1.0–3.3	0.5–5.4	7.8	1.1–2.3	0.7–3.0	0.3–5.2	7.6
2150	3.1–5.9	2.4–7.6	1.5–12.8	19.4	1.9–4.5	1.2–5.9	0.4–11.0	17	1.5–3.7	1.0–5.2	0.4–10.9	16.7
2200	4.2–9.0	3.1–12.1	1.9–21.8	33.3	2.2–6.5	1.2–9.3	-0.2–18.7	29.7	1.6–5.4	0.8–8.3	0.1–18.6	29.1
GRAND ISLE, LA												
2030	1.1–1.4	1.0–1.5	0.8–1.6	1.7	1.1–1.3	0.9–1.4	0.8–1.6	1.7	1.0–1.4	0.9–1.5	0.8–1.7	1.8
2050	1.9–2.4	1.7–2.6	1.5–3.0	3.5	1.8–2.3	1.7–2.4	1.5–2.8	3.3	1.8–2.3	1.6–2.5	1.4–2.8	3.3
2100	4.1–5.8	3.6–6.5	2.9–8.6	11.5	3.7–5.0	3.3–5.6	2.7–7.7	10.1	3.4–4.6	3.0–5.3	2.6–7.5	9.9
2150	6.6–9.4	5.8–11.1	4.9–16.3	22.9	5.4–7.9	4.7–9.4	3.8–14.5	20.6	4.9–7.1	4.5–8.7	3.9–14.3	20.2
2200	8.8–13.6	7.7–16.8	6.5–26.6	38.1	6.8–11.2	5.7–13.9	4.3–23.3	34.5	6.1–10.0	5.4–13.0	4.6–23.2	33.9
GALVESTON, TX												
2030	0.8–1.1	0.7–1.2	0.6–1.4	1.5	0.8–1.1	0.7–1.2	0.6–1.3	1.4	0.8–1.1	0.7–1.2	0.5–1.4	1.5
2050	1.5–2.0	1.3–2.2	1.1–2.6	3.1	1.4–1.8	1.3–2.0	1.1–2.3	2.8	1.4–1.8	1.2–2.0	1.0–2.4	2.9
2100	3.2–4.9	2.7–5.7	2.0–7.6	10.6	2.8–4.1	2.4–4.7	1.9–6.8	9.2	2.5–3.8	2.1–4.4	1.6–6.7	9.0
2150	5.3–8.1	4.6–9.8	3.6–15.0	21.5	4.1–6.6	3.4–8.1	2.5–13.1	19.2	3.7–5.9	3.2–7.4	2.6–13.0	18.8
2200	7.2–12.0	6.0–15.1	4.8–24.8	36.1	5.1–9.4	4.0–12.1	2.7–21.5	32.5	4.4–8.3	3.7–11.2	2.9–21.4	31.9

Table A15: Sea-level rise projections (con't)

Feet above 2000	RCP 8.5				RCP 4.5				RCP 2.6			
	Likely	90% range	99% range	1-in-1000	*Likely*	90% range	99% range	1-in-1000	*Likely*	90% range	99% range	1-in-1000
SAN DIEGO, CA												
2030	0.4–0.6	0.3–0.6	0.2–0.7	0.8	0.3–0.6	0.3–0.6	0.1–0.8	0.8	0.4–0.6	0.3–0.6	0.2–0.8	0.8
2050	0.7–1.2	0.6–1.3	0.4–1.7	2.3	0.7–1.1	0.5–1.2	0.3–1.6	2.1	0.6–1.0	0.5–1.2	0.3–1.6	2.1
2100	1.9–3.4	1.5–4.1	1.0–6.3	9.1	1.4–2.7	1.0–3.3	0.5–5.5	8	1.2–2.3	0.9–3.0	0.5–5.3	7.8
2150	3.1–5.9	2.4–7.7	1.7–13.0	19.6	2.0–4.5	1.4–6.1	0.5–11.2	17.6	1.6–3.8	1.1–5.3	0.6–11.0	17.1
2200	4.2–9.2	3.0–12.6	1.7–22.5	34	2.4–6.8	1.3–9.6	0.0–19.2	30.4	1.7–5.6	0.9–8.6	0.2–19.0	30
SAN FRANCISCO, CA												
2030	0.3–0.5	0.3–0.6	0.2–0.7	0.8	0.3–0.5	0.2–0.6	0.1–0.8	0.8	0.3–0.5	0.3–0.6	0.2–0.7	0.8
2050	0.7–1.1	0.5–1.3	0.3–1.6	2.3	0.6–1.0	0.5–1.2	0.3–1.5	2.1	0.6–1.0	0.4–1.1	0.2–1.5	2.1
2100	1.8–3.2	1.4–4.0	0.8–6.2	9	1.3–2.6	1.0–3.2	0.5–5.4	7.9	1.1–2.3	0.8–2.9	0.4–5.2	7.7
2150	2.9–5.7	2.3–7.5	1.5–12.9	19.4	1.9–4.4	1.2–5.9	0.4–11.1	17.4	1.4–3.6	1.0–5.2	0.5–10.9	17
2200	3.9–9.0	2.8–12.3	1.5–22.2	33.8	2.2–6.6	1.1–9.3	-0.1–19.1	30.3	1.5–5.4	0.7–8.4	0.0–18.9	29.9
ASTORIA, OR												
2030	0.1–0.3	0.0–0.3	-0.1–0.4	0.5	0.1–0.3	0.0–0.3	-0.1–0.5	0.5	0.1–0.3	0.0–0.3	-0.1–0.4	0.5
2050	0.2–0.6	0.1–0.8	-0.1–1.2	1.8	0.2–0.6	0.1–0.7	-0.1–1.1	1.6	0.2–0.6	0.0–0.7	-0.1–1.1	1.6
2100	1.0–2.3	0.6–3.0	0.1–5.3	7.9	0.5–1.7	0.2–2.3	-0.2–4.5	6.9	0.3–1.5	0.0–2.1	-0.4–4.4	6.8
2150	1.6–4.2	0.9–5.9	0.2–11.1	17.8	0.7–3.1	0.0–4.6	-0.7–9.7	15.8	0.3–2.4	-0.2–4.0	-0.6–9.6	15.5
2200	2.1–7.0	1.0–10.1	-0.3–19.8	31.5	0.6–4.8	-0.4–7.5	-1.6–17.2	28.2	-0.1–3.8	-0.8–6.7	-1.5–17.1	27.7
SEATTLE, WA												
2030	0.3–0.5	0.2–0.5	0.2–0.6	0.7	0.3–0.5	0.2–0.5	0.1–0.7	0.7	0.3–0.5	0.2–0.5	0.1–0.6	0.7
2050	0.6–1.0	0.5–1.1	0.3–1.5	2.1	0.6–0.9	0.4–1.1	0.2–1.4	1.9	0.5–0.9	0.4–1.1	0.2–1.4	1.9
2100	1.6–3.0	1.3–3.7	0.8–5.9	8.5	1.3–2.4	0.9–3.0	0.5–5.2	7.5	1.1–2.2	0.7–2.8	0.3–5.1	7.4
2150	2.6–5.2	2.0–6.9	1.3–12.0	18.6	1.8–4.1	1.1–5.6	0.3–10.7	16.6	1.3–3.4	0.9–5.0	0.5–10.6	16.3
2200	3.5–8.3	2.4–11.3	1.2–21.0	32.4	2.1–6.2	1.0–8.9	-0.2–18.4	29.1	1.4–5.2	0.7–8.1	0.0–18.3	28.6
JUNEAU, AK												
2030	-1.2–-1.1	-1.3–-1.0	-1.4–-0.9	-0.8	-1.2–-1.1	-1.3–-1.0	-1.4–-0.9	-0.8	-1.2–-1.1	-1.3–-1.0	-1.4–-0.9	-0.8
2050	-1.9–-1.6	-2.1–-1.5	-2.2–-1.1	-0.5	-2.0–-1.7	-2.1–-1.5	-2.2–-1.2	-0.7	-2.0–-1.7	-2.2–-1.5	-2.3–-1.2	-0.7
2100	-3.5–-2.4	-3.9–-1.7	-4.3–0.6	3.2	-3.9–-2.8	-4.2–-2.2	-4.6–-0.1	2.2	-4.1–-3.0	-4.4–-2.4	-4.7–-0.2	2.2
2150	-5.2–-2.6	-5.9–-1.0	-6.8–4.2	10.8	-6.0–-3.8	-6.6–-2.3	-7.3–2.9	8.6	-6.4–-4.3	-6.8–-2.7	-7.2–2.9	8.6
2200	-7.0–-2.3	-8.2–0.7	-9.5–10.3	22.1	-8.3–-4.4	-9.3–-1.6	-10.4–8.1	18.4	-8.8–-5.1	-9.6–-2.2	-10.3–8.2	18.3
ANCHORAGE, AK												
2030	-0.1–0.3	-0.2–0.4	-0.4–0.6	0.8	-0.1–0.4	-0.3–0.5	-0.5–0.8	0.9	-0.1–0.2	-0.2–0.4	-0.4–0.6	0.7
2050	-0.2–0.5	-0.4–0.8	-0.7–1.2	1.7	-0.2–0.6	-0.4–0.8	-0.8–1.3	1.6	-0.2–0.4	-0.4–0.7	-0.7–1.0	1.5
2100	-0.6–1.2	-1.2–2.0	-2.0–4.0	6.8	-0.3–1.3	-0.8–2.0	-1.5–3.9	6.5	-0.2–1.2	-0.6–1.8	-1.2–3.9	6.5
2150	-1.5–2.3	-2.7–4.2	-4.5–9.2	16	-0.5–2.4	-1.4–4.0	-2.7–8.9	15.1	-0.4–2.2	-1.2–3.8	-2.5–9.3	15.2
2200	-1.3–4.5	-3.0–7.5	-5.3–17.0	29.2	-0.5–4.2	-1.8–6.9	-3.5–16.4	27.4	-0.4–4.1	-1.6–7.1	-3.6–17.1	28
HONOLULU, HI												
2030	0.4–0.6	0.3–0.7	0.2–0.8	0.9	0.4–0.6	0.3–0.7	0.2–0.8	0.9	0.4–0.6	0.3–0.7	0.2–0.8	0.9
2050	0.8–1.2	0.6–1.4	0.4–1.9	2.5	0.7–1.1	0.6–1.3	0.4–1.7	2.2	0.6–1.1	0.5–1.3	0.3–1.7	2.2
2100	2.1–3.8	1.6–4.6	0.9–6.9	10	1.5–2.8	1.1–3.5	0.6–5.8	8.7	1.2–2.5	0.9–3.2	0.4–5.6	8.5
2150	3.3–6.6	2.4–8.7	1.4–14.3	21.5	2.1–4.9	1.3–6.5	0.4–12.0	19	1.5–4.0	1.0–5.7	0.5–11.7	18.6
2200	4.4–10.4	2.9–14.2	1.3–24.8	37.7	2.4–7.3	1.2–10.4	-0.3–20.5	33.2	1.6–6.1	0.7–9.3	-0.1–20.0	32.8

Collins, M., R. Knutti, and et al. (2013), Chapter 12: Long-term climate change: Projections, commitments and irreversibility, in *Climate Change 2013: the Physical Science Basis*, edited by T. F. Stocker, D. Qin, G.-K. Plattner, M. Tignor, S. K. Allen, J. Boschung, A. Nauels, Y. Xia, V. Bex, and P. Midgley, Cambridge University Press.

Davies-Jones, R. (2008), An efficient and accurate method for computing the wet-bulb temperature along pseudoadiabats, *Monthly Weather Review*, *136*(7), 2764–2785, doi:10.1175/2007MWR2224.1.

Doswell, C. A., III, J. T. Schaefer, D. W. M. T. W. Schlatter, and H. B. Wobus (1982), Thermodynamic analysis procedures at the National Severe Storms Forecast Center, in *Ninth Conference on Weather Forecasting and Analysis*, pp. 304–309, American Meterological Society, Seattle, WA.

Gomez, N., D. Pollard, J. X. Mitrovica, P. Huybers, and P. U. Clark (2012), Evolution of a coupled marine ice sheet–sea level model, *Journal of Geophysical Research*, *117*, F01,013, doi:10.1029/2011JF002128.

Gomez, N., D. Pollard, and J. X. Mitrovica (2013), A 3-D coupled ice sheet – sea level model applied to Antarctica through the last 40 ky, *Earth and Planetary Science Letters*, *384*, 88–99, doi:10.1016/j.epsl.2013.09.042.

Joughin, I., B. E. Smith, and B. Medley (2014), Marine ice sheet collapse potentially underway for the Thwaites Glacier Basin, West Antarctica, *Science*, *344*, 735–738, doi:10.1126/science.1249055.

Konikow, L. F. (2011), Contribution of global groundwater depletion since 1900 to sea-level rise, *Geophysical Research Letters*, *38*, L17,401, doi:10.1029/2011GL048604.

Kopp, R. E. (2013), Does the mid-Atlantic United States sea level acceleration hot spot reflect ocean dynamic variability?, *Geophysical Research Letters*, *40*, 3981–3985, doi:10.1002/grl.50781.

Kopp, R. E., R. M. Horton, C. M. Little, J. X. Mitrovica, M. Oppenheimer, D. J. Rasmussen, B. H. Strauss, and C. Tebaldi (2014), Probabilistic 21st and 22nd century sea-level projections at a global network of tide gauge sites, *Earth's Future*, doi:10.1002/2014ER000239.

Little, C. M., M. Oppenheimer, and N. M. Urban (2013), Upper bounds on twenty-first-century Antarctic ice loss assessed using a probabilistic framework, *Nature Climate Change*, *3*, 654–659, doi:10.1038/nclimate1845.

Marsh, P. T., and J. A. Hart (2012), SHARPPY: A Python Implementation of the Skew-T/Hodograph Analysis and Research Program, in *92nd American Meteorological Society Annual Meeting*, American Meteorological Society, New Orleans, LA.

Marzeion, B., A. H. Jarosch, and M. Hofer (2012), Past and future sea-level change from the surface mass balance of glaciers, *The Cryosphere*, *6*, 1295–1322, doi:10.5194/tc-6-1295-2012.

Maurer, E. P., A. W. Wood, J. C. Adam, D. P. Lettenmaier, and B. Nijssen (2002), A long-term hydrologically based dataset of land surface fluxes and states for the conterminous United States, *Journal of Climate*, *15*(22), 3237–3251.

Meinshausen, M., N. Meinshausen, W. Hare, S. C. Raper, K. Frieler, R. Knutti, D. J. Frame, and M. R. Allen (2009), Greenhouse-gas emission targets for limiting global warming to 2 C, *Nature*, *458*(7242), 1158–1162, doi:10.1038/nature00817.

Meinshausen, M., S. C. B. Raper, and T. M. L. Wigley (2011), Emulating coupled atmosphere-ocean and carbon cycle models with a simpler model, MAGICC6 – Part 1: Model description and calibration – Part 1: Model description and calibration, *Atmos. Chem. Phys.*, *11*(4), 1417–1456, doi:10.5194/acp-11-1417-2011.

Mesinger, F., G. DiMego, E. Kalnay, K. Mitchell, P. C. Shafran, W. Ebisuzaki, D. Jović, J. Woollen, E. Rogers, E. H. Berbery, et al. (2006), North American regional reanalysis, *Bulletin of the American Meteorological Society*, *87*(3), 343–360, doi:10.1175/BAMS-87-3-343.

Miller, K. G., R. E. Kopp, B. P. Horton, J. V. Browning, and A. C. Kemp (2013), A geological perspective on sea-level rise and impacts along the U.S. mid-Atlantic coast, *Earth's Future*, *1*, 3–18, doi:10.1002/2013EF000135.

Mitchell, T. D. (2003), Pattern scaling: an examination of the accuracy of the technique for describing future climates, *Climatic Change*, *60*(3), 217–242, doi:10.1023/A:1026035305597.

Pollard, D., and R. M. DeConto (2013), Modeling drastic ice retreat in Antarctic subglacial basins, in *AGU Fall Meeting Abstracts*, Abstract GC34A-03, San Francisco, CA.

Rignot, E., J. Mouginot, M. Morlighem, H. Seroussi, and B. Scheuchl (2014), Widespread, rapid grounding line retreat of Pine Island, Thwaites, Smith, and Kohler glaciers, West Antarctica, from 1992 to 2011, *Geophysical Research Letters*, *41*, 3502–3509, doi:10.1002/2014GL060140.

Rogelj, J., M. Meinshausen, and R. Knutti (2012), Global warming under old and new scenarios using IPCC climate sensitivity range estimates, *Nature Climate Change*, *2*(4), 248–253, doi:10.1038/nclimate1385.

Schoof, C. (2007), Ice sheet grounding line dynamics: Steady states, stability, and hysteresis, *Journal of Geophysical Research*, *112*(F3), F03S28, doi:10.1029/2006JF000664.

Sherwood, S., and Q. Fu (2014), A drier future?, *Science*, *343*(6172), 737–739, doi:10.1126/science.1247620.

Tebaldi, C., and R. Knutti (2007), The use of the multi-model ensemble in probabilistic climate projections, *Philosophical Transactions of the Royal Society A: Mathematical, Physical and Engineering Sciences*, *365*(1857), 2053–2075, doi:10.1098/rsta.2007.2076.

Wada, Y., L. P. H. van Beek, F. C. Sperna Weiland, B. F. Chao, Y.-H. Wu, and M. F. P. Bierkens (2012), Past and future contribution of global groundwater depletion to sea-level rise, *Geophysical Research Letters*, *39*, L09,402, doi:10.1029/2012GL051230.

Wood, A. W., E. P. Maurer, A. Kumar, and D. P. Lettenmaier (2002), Long-range experimental hydrologic forecasting for the eastern United States, *Journal of Geophysical Research: Atmospheres*, *107*(D20), 4429, doi:10.1029/2001JD000659.